Investigation of the causes of historical changes in the sub-surface salinity minimum of the South Atlantic

Marlos Goes,[1] Ilana Wainer,[2], and Natalia Signorelli[2]

Corresponding author: Marlos Goes, CIMAS/University of Miami and NOAA/AOML, Miami, USA. (marlos.goes@noaa.gov)

[1]CIMAS/University of Miami and

NOAA/AOML, Miami, USA.

[2]Institute of Oceanography, University of

São Paulo,São Paulo, Brazil

Abstract.

In this study we investigate the sub-surface salinity changes on decadal timescales across the Subtropical South Atlantic Ocean using two ocean re-analysis products, the latest version of the Simple Ocean Data Assimilation and the Estimating the Circulation and Climate of the Ocean, Phase II , as well as with additional climate model experiments. Results show that there is a recent significant salinity increase at the core of the salinity minimum at intermediate levels. The main underlying mechanism for this sub-surface salinity increase is the lateral advective (gyre) changes due to the Southern Annular mode variability, which conditions an increased contribution from the Indian Ocean high salinity waters into the Atlantic. The global warming signal has a secondary but complementary contribution. Latitudinal differences at intermediate depth in response to large-scale forcing are in part caused by local variation of westward propagation features, and by compensating contributions of salinity and temperature to density changes.

1. Introduction

Modulation and stability of the South Atlantic meridional overturning circulation are dependent on salinity changes [*Weijer et al.*, 2002; *Peeters et al.*, 2004], and an improved understanding of the mechanisms behind these salinity variations, especially the signature of change below the ocean surface, is essential for better monitoring and prediction of long-term climate change.

Long-term changes in ocean salinity are a function of large scale atmospheric forcing as well as regional freshwater fluxes. In the South Atlantic Ocean, significant ocean warming, which drives trends in freshwater fluxes, has been documented from observations and is the subject of much research [*Gille*, 2002; *Curry et al.*, 2003; *Boyer et al.*, 2005; *Grodsky et al.*, 2006; *Böning et al.*, 2008; *Schmidtko and Johnson*, 2012; *McCarthy et al.*, 2012]. Ocean salinity changes are in general depth and latitudinally dependent [*Curry et al.*, 2003]. They are larger in the top 500 m of the ocean because of the direct effect of atmospheric fluxes. In comparison to earlier data on record (1960–1970s), more recent years (1990s) have shown salinity increases in the tropical-subtropical latitudes due to warming and increased evaporation [*Boyer et al.*, 2005], and salinity decreases in the extratropical regions due to enhanced precipitation and runoff (including ice melting).

However, these long-term changes are subject to intense interannual and decadal variability [*Grodsky et al.*, 2006], and more recent data show an actual decrease in surface salinity in the tropical Atlantic due to increased precipitation and upwelling. This impacts the mixed layer depth, and therefore the formation of subsurface water masses.

Water masses that are formed on the base of the mixed layer are in contact with the atmosphere for a relatively short period during their formation. They are eventually subducted into the ocean interior following mostly an adiabatic pathway along neutral density surfaces. At depth they are also modified by mixing which acts on much longer timescales. Below the surface, the signature of salinity changes in the ocean is subject to higher uncertainty than at the surface, since salinity is dynamically entangled with the temperature field, which together determine the density [*Pierce et al.*, 2012]. Therefore, understanding salinity changes in the South Atlantic at intermediate depths requires understanding the relative contribution of the associated processes [*Durack and Wijffels*, 2010], such as surface atmospheric forcing, circulation changes, changes due to mixing along the water-mass pathways, and vertical movements of isopycnals due to wind field effects.

In the South Atlantic, an important impact of atmospheric forcing can be related to changes in the Southern Annular Mode (SAM) through variations in sea level pressure (SLP), which in turn would impact on the surface wind leading to a broad-scale surface warming associated with the poleward migration of isopycnal outcrops [*Durack and Wijffels*, 2010; *Schmidtko and Johnson*, 2012].

Although frequent in situ salinity data are scarce in the South Atlantic before 2002, several studies have used historical ship-based conductivity– temperature–depth (CTD) along with more recent Argo floats data to investigate long-term changes in the Sub-Antarctic Mode Water (SAMW) and in the Antarctic Intermediate Water (AAIW) salinity minimum layer underneath. Analysis of these data indicate cooling and freshening of the SAMW, and warming and salinification associated with the AAIW [*Bindoff and*

McDougall, 1994; Böning et al., 2008; McCarthy et al., 2011; Schmidtko and Johnson, 2012]. Results also show a statistically significant shoaling of the isopycnals within the circumpolar AAIW, accompanying a decrease in density, and an equatorward spreading of the salinity anomalies at the sub-surface [Durack and Wijffels, 2010; Schmidtko and Johnson, 2012]. A further decrease in the AAIW density is also projected for the 21st century in climate models [Goes et al., 2008].

Further analysis of Argo observations reveals the variability of the AAIW salinity in the South Atlantic on interannual and intradecadal timescales. Westward propagating salinity anomalies at 30°S show that Rossby wave mechanisms are important for the interpretation of salinity changes associated with the hydrological cycle of the AAIW at these timescales [McCarthy et al., 2012].

In this study we investigate changes in the sub-surface salinity minimum of the South Atlantic and its relation to large-scale trends such as those related to global warming via greenhouse gases and the Southern Annular Mode (SAM). For this we use a blend of ocean reanalyses and process oriented climate model experiments.

This paper is outlined as follows: Section 2 describes the two ocean reanalyses used in this study; Section 3 shows the results of the examination of the two reanalysis data, followed by the analysis of the climate model experiments. The setup of the climate model experiments is presented in an Appendix; Sections 4 and 5 contain a discussion of the results and the conclusion of this study.

2. Data

The first part of this study utilizes temperature and salinity data from the Simple Ocean Data Assimilation (SODA) version 2.2.6 [Ray and Giese, 2012], and from the Estimating

the Circulation and Climate of the Ocean, Phase II (ECCO2). They can be described as follows:

2.1. SODA 2.2.6

SODA 2.2.6 uses the Parallel Ocean Program (POP) model [*Smith et al.*, 1992] at a 1/4° horizontal resolution, which is publicly available at an interpolated 0.5° x 0.5° horizontal resolution, and 40 vertical levels at monthly averages, spanning the period of 1871 to 2008. Vertical diffusion of momentum, heat, and salt are carried out using K-profile parameterization (KPP) mixing with modifications to address issues such as diurnal heating, while lateral subgrid-scale processes are modeled using biharmonic mixing.

Surface boundary conditions used are from eight ensemble members of the NOAA atmospheric Twentieth Century reanalysis 20Crv2 [*Compo et al.*, 2011]. SODA 2.26 assimilates only sea surface temperature (SST) data using a sequential estimation data assimilation method [*Carton and Giese*, 2008]. The SST data comes from the ICOADS 2.5 SST product (http://icoads.noaa.gov), which is based solely on in-situ observations (e.g., XBT, CTD, bottle, Argo) and reached 2 million data reports per year in the 1960s. Heat and salt fluxes in SODA are calculated from bulk formulae using 20CRv2 daily variables. By not assimilating in-depth hydrography and only SST, the model is more dynamically consistent over different decades than alternative versions. A complete overview of the ocean-reanalysis process is detailed by *Carton and Giese* [2008].

2.2. ECCO2

The Estimating the Circulation and Climate of the Ocean, Phase II (ECCO2) project [*Menemenlis*, 2008]. An ECCO2 data synthesis is obtained by least-squares fit of a global

full-depth-ocean and sea-ice configuration of the Massachusetts Institute of Technology OGCM [*Marshall et al.*, 1997] to the available satellite and in situ data. This least-squares fit is carried out for a small number of control parameters using a Green's function approach [*Menemenlis*, 2005]. The solution requires the computation of a number of sensitivity experiments that are free, unconstrained calculations by a forward model. The experiments are designed to adjust the model parameters, forcing, and initial conditions. Then the model is run forward again using the adjusted parameters, free of any constraints, as in any ordinary model simulation. The model employs a cube-sphere grid projection with a mean horizontal grid spacing of 18 km and 50 vertical levels. Surface forcings such as wind and precipitation are from the JRA25 reanalysis [*Onogi*, 2007]. In the present work, we use monthly average fields from January 1992 to December 2012.

3. Results

3.1. AAIW properties in SODA and ECCO2

As stated in the previous section, SODA 2.2.6 assimilates only SST data. This allows the model to be more dynamically consistent over time, although larger differences may exist with respect to actual hydrographic data. Salinity data in the South Atlantic are historically sparse, mostly available in a more consistent way since the 2000s from Argo floats measurements. ECCO2 uses a Green functions method, which also allows a smooth salinity path over time, and allows a stronger hydrographic constraint with depth. We estimate the differences in the representation of the AAIW in both reanalyses by comparing their salinity properties with an Argo climatology [*Roemmich and Gilson*, 2009], which is available at a 1 degree horizontal resolution starting in 2004, for a similar period. The Argo climatology exhibits a minimum salinity tongue in the central basin (at

25°W; Figure 1c) extending from its formation region (between 45 and 60°S) across the

mixed layer to a maximum depth of 600–1200 m at 35-40°S. The salinity minimum follows

closely the depth of the isopycnal $\sigma_\theta = 27.2$ kg/m^3, which is approximately 1000 m deep

in this region. Previous studies have associated the depth of the salinity minimum with

the $\sigma_\theta = 27.2$ kg/m^3 isopycnal surface, and also with the neutral density surface $\gamma_n = 27.4$

kg/m^3 [*You*, 2002]. North of 20°S, the $\sigma_\theta = 27.2$ kg/m^3 density surface levels out to a

depth of 700 m, and the salinity minimum flows underneath a salty surface region of

maximum evaporation minus precipitation (E-P).

The features revealed in SODA resemble the ones from the observations over a similar

period (i.e., 2004–2009; Figure 1a). In SODA, the isopycnals south of 40°S are much more

tilted than observations, and the maximum depth of the $\sigma_\theta = 27.2$ kg/m^3 is approximately

1200 m deep, 200 m deeper than the observations. The salinity minimum in the South

Atlantic is also deeper in SODA than in the observations. This causes a maximum anomaly

of salinity on 40°S of up to 0.6 psu at 500 m depth (Figure 1d). At ∼7°S, SODA shows a

strong near-surface upwelling region, characterized by an uplifting of the isopycnals. This

feature is not evident in the ARGO climatology. ECCO2 results show that the minimum

salinity is well constrained, with a maximum depth at approximately 800 m, and the

differences of salinity with depth are therefore much reduced (< 0.2 psu) in comparison

to SODA (Figure 1e).

Next, we compare the regional features of the salinity minimum in the South Atlantic

between the reanalyses and Argo, doing so after interpolating all products to the Argo

resolution. The salinity minimum surface in the South Atlantic is shown in Figure 2.

SODA shows a stronger Subantarctic Front (SAF; ∼ 45 °S) than in observations (Figure

147 2a, c), which agrees with the larger isopycnal slopes in that region, as revealed in Figure

148 1a. For this reason the SAF region shows the largest salinity differences (~ 0.3) between

149 SODA and Argo (Figure 2d). In the other regions salinity differences are smaller, and can

150 reach approximately 0.1 in magnitude. ECCO2 (Figure 2b) shows a better representation

151 of the SAF region relative to SODA, and the biases are below 0.15 psu in the region.

152 North of 30°S, biases in ECCO2 and SODA show similar magnitudes. Although there

153 are differences within the two reanalysis products, which are based on different models,

154 assimilation methods and observations assimilated, and between the reanalysis products

155 and observations, similar results in terms of their temporal and spatial variability will

156 lend credence to the robustness of the variability of the AAIW in the region.

3.2. Regional trends in the AAIW

157 In the South Atlantic, changes in the relationship of temperature and salinity along

158 isopycnals show latitudinal dependence. The time and latitude distribution of the South

159 Atlantic salinity at various density levels from the 1960s to 2000s is here inferred from

160 Temperature-Salinity (θ/S) diagrams for four latitudes (35°S, 30°S, 20°S, 10°S; Figure 3).

161 At 35°S (Figure 3a), SODA (solid lines) show strong salinity variability in the ther-

162 mocline waters. Salinity values are higher in the 2000s, although this increase is not

163 monotonic over time, instead alternating, with the 1970s and 1990s having lower salinity

164 values, and the 1960s, 1980s and 2000s having higher salinity values. Similar alternating

165 patterns are found along 30°S and 10°S (Figures 3b and 3d, respectively). At 10°S, which

166 is located in the tropical region of high E-P, salinity increases by 0.2 in the upper tropical

167 waters, which is related an enhanced hydrological cycle in the region [*Curry et al.*, 2003;

168 *Helm et al.*, 2010]. At 20°S (Figure 3c), the 2000s SODA shows lower salinity values at the

thermocline, and higher values in the 1970s. The smallest differences in θ/S over time are found at 20°S for the whole profile. The central and intermediate water levels generally have opposing signs of changes at all latitudes. Central waters show a recent cooling and freshening along isopycnals, as is apparent in the density layer between $\sigma = 26.5$ and 27.0 kg m^{-3}, whereas intermediate waters generally show warming and increased salinity between $\sigma = 27.2$ and 27.4 kg m^{-3} (highlighted in the insets of Figure 3). Central water freshening has been suggested to be related to changes in subduction processes at this density range [*Durack and Wijffels*, 2010]. ECCO2 (dashed lines) shows higher surface salinities than SODA in the thermocline, especially at higher latitudes (Figures 3a, b), and generally lower salinity values in intermediate levels. Salinity changes in ECCO2, however, agree with SODA in that there is a salinity increase in the thermocline and intermediate layers, and a decrease in the central water layers.

The spatial distribution of salinity minimum trends in SODA and ECCO2 are shown in Figures (4a, b). For consistency, the trends are calculated since 1992 for the two products. SODA and ECCO2 show an increase in the salinity minimum since 1992 almost everywhere in the South Atlantic.

To investigate how the trends in the dynamical parameters at the salinity minimum position observed in Figures (4a,b) are significant over time, we produce a time series of the salinity, potential density (σ_θ) and temperature anomalies for SODA and ECCO2 relative to the SODA's average over its whole time series period at the depth of the salinity minimum. We consider two locations in the central part of the basin, at 25°W/30°S and 25°W/35°S (Figure 4). At both latitudes, SODA (black line) shows an increase in salinity and temperature in the late 1980s/beginning of 1990s until the end of the series (Figure

192 4c,g,d,h). This joint effect of warming and salinification produces a reduction in density

193 during this period (Figure 4e,f); a feature that agrees with climate projections of the

194 AAIW [*Goes et al.*, 2008]. The effect of the density decrease at the minimum salinity

195 depth is more prominent at 35°S than at 30°S. There is strong decadal variability at both

196 latitudes, although fluctuations appear in different periods: at 30°S, there is a general

197 freshening trend from the 1960s to the 1970s, and an increase in salinity after 1976 (Figure

198 4c). The rate of salinity increase from the mid-1970s to the mid-1990s is the highest with

199 about 0.01 per decade, while it levels out considerably in the late 1990s and 2000s.

200   At 35°S there is a significant positive salinity anomaly in the 1970s, followed by an also

201 significant negative salinity anomaly in the 1980s. A linear trend of about 0.05 per decade

202 is apparent after that. Trends observed in SODA after 2000 in all analyzed parameters

203 exceed 3 standard deviations (red dashed lines in Figure 4) calculated for the whole time

204 series period, showing that these trends are likely to be statistically significant. Timeseries

205 of ECCO2 (blue lines) for temperature, salinity and density show much stronger variability

206 than found SODA, which makes the detection of salinity changes since 1992 more difficult.

207 However, property changes in ECCO2 compares well with the ones from SODA for the

208 same period.

209   The interannual-to-decadal salinity changes shown in Figure (4) are consistent with re-

210 cent findings that changes in the rate of global surface temperature increase have occurred

211 in previous decades, such as in the mid-1970s [*Levinson and Lawrimore*, 2008; *Trenberth*

212 *and Coauthors*, 2007], and that these changes can potentially produce signals in density

213 and salinity at depth [*Durack and Wijffels*, 2010].

3.3. Density changes in the subtropical Atlantic

According to *Bindoff and McDougall* [1994], salinity changes at depth have three main causes: i) freshening/salinification on isopycnals, ii) warming/cooling on isopycnals and iii) heave, which is related to vertical displacements of isopycnals without changes in salinity and temperature. Therefore, knowledge of these salinity changes requires understanding the causes of density changes at intermediate levels.

Timeseries in Figure 4 suggest that there is compensation between temperature and salinity at the salinity minimum depth. An increase in salinity, which forces an increase in density, is accompanied by an increase in temperature, and consequently a decrease in density.

We investigate the causes of variability of density around the salinity minimum depth ($\sim$1000 m) by estimating the thermopycnal and halopycnal changes at that depth. For this we keep the salinity or temperature constant at their climatological mean values, and let the other component vary over time. This way, we are able to estimate the main contribution of density changes, which drive the large-scale meridional water displacement in the ocean.

The correlation between the thermopycnal and halopycnal terms provide information of the compensation between them (Figure 5). If the components are highly negatively correlated, strong compensation is diagnosed. In opposition, weak or positive correlation means that one of the terms is probably controlling the density changes. SODA and ECCO2 show that there are dominant regions of compensation. Compensation occurs mostly in the middle of the subtropical gyre, where correlation between the thermal and haline terms are often below -0.7. In the regions that compensation happens, the individ-

ual components have weak correlation with density (not shown), therefore no contribution is dominant. North of 30°S, the two components are positively correlated, and in this part of the domain temperature is a stronger driver of density changes.

This compensating behavior can explain the larger variability of salinity values on isopycnals at 35°S than at 30°S, shown in Figure 4. Other studies have found similar compensating patterns in the North Atlantic [*Lozier et al.*, 2010], where compensation on decadal timescales is associated with water mass changes, rather than heave mechanisms. Since ECCO2 reanalysis only spans for two decades, which would hinder our ability to meaningfully interpret its changes as a part of a longer-term trend, we use SODA 2.2.6 to infer how salinity and gyre changes are inter-related in the South Atlantic.

3.4. Subtropical Gyre variability in SODA

An AAIW layer, which encompasses the the salinity minimum surface depths ($\sim$ 800–1100 m), is constructed by defining two neutral density surfaces [*Jackett and McDougall*, 1997] as the upper and lower boundaries, the $\gamma_n = 27.1$ and $\gamma_n = 27.6$, respectively. Within this layer (Figure 6a), there is a signature of the inflow of salty Indian Ocean waters through the southeastern tip of the Atlantic. The high salinity Indian Ocean waters at intermediate levels are formed in the Red Sea [*Talley*, 2002], and flow into the Agulhas Current through the Mozambique Channel. While entering the South Atlantic, the mixing with the AAIW low salinity waters modify the Red Sea water along its trajectory northwestward. It has been estimated that approximately 50% of the Benguela Current waters at intermediate levels are formed in the Indian Ocean [*Gordon et al.*, 1992]. The low salinity AAIW waters are originated in large extent in the southeastern Pacific [*McCartney*, 1977; *Saenko et al.*, 2003] and flow eastward along the sub-Antarctic front

258 (SAF). The AAIW follows a path similar to the one predicted by the ventilated thermo-

259 cline theory [*Schmid et al.*, 2000], and a "shadow zone" is formed in the northeast part

260 of the South Atlantic, which also contains relatively high salinity values. From Figure

261 6a, a minimum on the salinity minimum surface is obvious at about 30°S (Figure 6a),

262 crossing the basin from east to west following the Benguela Current Extension [*Schmid*

263 *and Garzoli*, 2009], which feeds into the Brazil Current (BC) along the western bound-

264 ary. BC waters encounter the Malvinas Current waters between 35°S and 40°S, resulting

265 in a westward inflow of low salinity waters along the South Atlantic Current [*Goni and*

266 *Wainer*, 2001; *Wainer et al.*, 2000].

267 SODA shows decadal changes in salinity between the 1960 and 2000 (Figure 6b–e).

268 Compared to the 1960s, the 1970s and the 1980s show a slight decrease in the minimum

269 salinity in most parts of the South Atlantic. A noticeable feature in the 1970s and later

270 in the 1990s and 2000s is the southward shift of the Brazil-Malvinas confluence up to

271 approximately 3 degrees, in comparison to the 1960s. This shift produces positive salinity

272 anomalies north and negative south of 35°S in the western part of the basin. In opposition,

273 the 1980s (Figure 6c) show a northward migration of the confluence, which can explain

274 some of the decadal variability shown in Figures (4d,h).

275 The 1990s show reduced salinity in the center of the salinity minimum south of 35°S,

276 and a general increase of salinity in the rest of the basin. These changes agree with results

277 from *Schmidtko and Johnson* [2012], in that negative salinity trends are observed in this

278 region over the past 50 years, although these trends are not statistically significant.

279 Of great importance is the enhanced inflow of higher salinity waters from the Agulhas

280 Current retroflection region in the southeastern part of the basin, which increases the

signature of these waters toward the northwestern part of the basin. In the 2000s (Figure 6e), this positive salinity trend in the basin continues, and increased salinity values are also found on the western side of the basin. This can have implications for the interhemispheric transport through the North Brazil Undercurrent, as shown in [*Biastoch et al.*, 2008].

Advective mechanisms within the gyre have the potential to drive a large part of the salinity increase displayed in SODA. This can be quantified with potential vorticity (PV) maps for the defined intermediate layer (Figure 7). The Ertel's PV is calculated as:

$$PV = \frac{f}{\rho_0} \frac{\Delta \gamma_n}{\Delta z} \tag{1}$$

where f is the Coriolis parameter, ρ_0 is the mean density of the ocean, $\Delta \gamma_n = 0.5$ kg m^{-3}, and Δz is the layer thickness.

The region is characterized by negative PV over the whole South Atlantic basin, characteristic of the planetary vorticity of the region (Figure 7a). The anticyclonic subtropical gyre is delimited by stronger negative vorticity (PV < -6 × 10^{-11}m^{-1}s^{-1}). From Figure 7 we can infer qualitatively the regions of high and low mixing. PV homogenization is generally characteristic of high mixing, whereas across PV fronts there is inhibited mixing, since they generate a barrier for the flow [*Beal et al.*, 2006]. The subtropical gyre is a natural path for the flow to enter the basin, and high mixing occurs along its path westward between 25-30°S.

The PV anomaly maps (Figure 7b–d) reveal that, starting in the 1980s, the PV in the AAIW layer has become more negative within the subtropical gyre. This suggests a spin-up of the anticyclonic gyre recently. Additionally, there has been an expansion of the negative gyre's PV southward, in agreement with observational results suggesting an expansion southward of the surface subtropical gyre [*Roemmich et al.*, 2007; *Goni et al.*,

2011], and a sectional poleward migration of the ACC [*Gille*, 2008]. This effect could potentially increase the mixing between Agulhas and South Atlantic waters in the eastern part of the basin. It would displace the minimum salinity region in the southwestern part of the salinity minimum surface to the south, promoting the increase of salinity north of this region.

The gyre strength and location are associated with the Sverdrup dynamics, therefore determined by the strength and location of the wind stress curl, respectively [*Lumpkin and Garzoli*, 2011]. Some properties of the wind stress in SODA are shown in Figure 8. Since 1960s there has been an overall increase in the westerlies strength in the eastern side of the basin, from 0.13 Pa to 0.16 Pa in the 2000s (Figure 8a). This effect is accompanied by a slight southward migration of the maximum wind stress curl (Figure 8b), from 38°S in the 1960s to 40°S in the 2000s, and an increase in the maximum wind stress curl from 19 Pa/m to 26 Pa/m (Figure 8c). In response to this forcing, according to the Sverdrup dynamics, there would be an extension of the gyre southwards that follows the latitude of the wind stress curl, and a spin up of the gyre, as a response to an increase in the wind stress curl. As we shall see, the magnitude of the westerlies in the eastern side of the basin affects the Agulhas leakage and the input of high salinity waters to the South Atlantic at intermediate levels.

3.5. Westward propagating Rossby Waves

As noted by *McCarthy et al.* [2012], salinity anomalies can be generated at intermediate depths in the eastern side of the basin, and propagate westward with a second mode Rossby wave speed. *McCarthy et al.* [2012] suggests that this can be an important mechanism to explain the variability of the salinity minimum across the basin on interannual timescales.

In Figure 6, there is a clear extension of the subtropical gyre and increase in the Agulhas leakage at intermediate depths.

The Agulhas leakage is well correlated with the strength of the westerlies [*Durgadoo et al.*, 2013] in the eastern part of the Atlantic basin. Similarly to *Durgadoo et al.* [2013], we define an index for the strength of the westerlies in the eastern part of the basin as the average zonal wind stress within 35°S–65°S and 0°W–20°E.

To investigate how salinity anomalies originated in the Agulhas leakage region are forced by the westerly winds and spread over the South Atlantic, we apply to SODA a lagged correlation of the westerly wind stress index in the eastern side of the basin to the salinity minimum surface. The time series are previously smoothed with a 9-month Boxcar window to filter the seasonal variability. The spatial distribution of the maximum lagged correlations and their associated lags are shown in Figure 9. The lag of the maximum correlation over space shows the propagation patterns of the salinity anomalies. Small lag values, close to zero or even negative, are observed in the eastern side of the basin. Negative lag values in the southeastern tip of the basin suggest that the flow in the Agulhas leakage is driven in great part by the wind stress anomalies east of Africa. Where the lag shows smaller values, the correlation of the westerlies and the salinity anomalies is highest, above 0.6. Anomalies propagate along a northwestern trajectory, following the ocean circulation at that depth (Figure 7a). This is also a characteristic pattern of the Rossby wave signal, which phase speed decreases poleward. The largest extension of the westward propagation of the salinity anomalies is observed along 29°S, which exhibits a time lag of approximately 120 months (10 years) to be completed. South of 30°S the lag increases considerably up to 200 months, i.e., about 17 years.

To investigate whether Rossby wave propagation is a plausible dynamical mechanism for the variability of the AAIW on interannual to decadal timescales, we examine time-longitude plots (Hovmoller diagrams) at two latitudes, 30°S and 35°S (Figure 10). Hovmoller diagrams allow us to determine zonal propagation patterns along a given latitude. In these diagrams, propagating waves appear as diagonal bands across the basin, and the slopes of these patterns are equal to the phase speed (c_p) of the waves. Here, wave characteristics are assessed objectively using the Radon Transform (RT) applied to the Hovmoller diagrams [*Challenor et al.*, 2001; *Polito and Liu*, 2003; *Barron et al.*, 2009]. This method rotates the coordinate system of the zonal-temporal diagrams in order to find the patterns that best align with the rotated axis.

The Hovmoller diagrams are for salinity anomalies (calculated with respect to the annual mean climatology) projected onto the $\gamma_n = 27.4$ neutral surface. Zonal means are subtracted from the anomalies field to filter decadal trends [*Barron et al.*, 2009], thus highlighting the interannual timescales. West-to-east propagating anomalies spread along 30°S. The optimal propagation speed is $cp = 1.79 \pm 0.48$ cm s^{-1}, at which anomalies travel across the basin in approximately 10 years. A similar result is obtained in the lag correlation maps shown in Figure 9. These speeds strongly agree with those obtained by *McCarthy et al.* [2012], who estimated a propagation speed of $cp = 1.7$ cm s^{-1}, which is characteristic of a second baroclinic mode wave propagation.

At 35°S, the situation is different. Propagation speeds of 0.47 ± 0.06 cm s^{-1} are much slower than the one predicted by the Rossby wave theory. In fact, the pattern of the variability in the eastern part of the basin (east of 15°W) seems to be unrelated to the one further west. From Figure 9, we observe that the correlations decrease considerably

from east to west at this latitude, and also the ability of the waters from the east to mix westward. Figure 7a shows that there is a strong gradient o PV around 35°S and 15°W, the approximate position of the change in the propagation pattern shown in Figure 10b. According to *Beal et al.* [2006], PV fronts are able to prevent mixing and advection along water masses trajectories. This effect may explain the low correlations of salinity anomalies in the western part of the basin at this latitude, and regional dynamics should play a larger role in this area.

To be assured, we performed additional calculations of the salinity propagation speeds using ECCO2 at the 30°S and 35°S. The values found for ECCO2 are 1.84 $\pm$0.45 and 0.46 $\pm$ 0.1 m/s, respectively, in large agreement with the speeds retrieved for SODA, showing that these results are robust across products.

3.6. Wind x CO_2

In the previous sections we show that SODA 2.2.6 exhibits changes in the subsurface salinity minimum and circulation patterns at intermediate layers. These changes include decadal variability overlapping a background low frequency variability, which becomes stronger after the 1970s. Other studies confirm that similar subsurface changes have occurred since 1950 [e.g., *Levitus et al.*, 2000; *Gille*, 2002; *Levitus et al.*, 2005; *Domingues et al.*, 2008; *Levitus et al.*, 2009; *Durack and Wijffels*, 2010; *Gille*, 2008; *Lyman et al.*, 2010].

In order to examine the possible causes of the salinity minimum variability, we perform idealized experiments with an Earth System Model of Intermediate Complexity in which two possible forcings, the wind stress curl changes in the Atlantic and the global warming due to CO_2 are separated. In these experiments, we use the University of Victoria Earth

System Model of Intermediate Complexity (UVic 2.9) [*Weaver et al.*, 2001]. This model

has been widely used in climate simulations and model comparison studies. We separate

the influences of the wind stress on the advective mechanisms in the South Atlantic into

northern and southern hemispheric forcings, by defining the first hemispheric modes of

variability, which are related to the North Atlantic Oscillation (NAO) and SAM, to the

north and south respectively. A description of the model experiments can be found in

Appendix A.

3.6.1. AAIW changes in the intermediate complexity model

Here, we analyze the response of the Atlantic salinity minimum surface to separate

atmospheric forcing, as described in Appendix A. Although UVic has a coarse resolution,

it can represent the salinity minimum surface below 200 m depth reasonably well (Figure

11a). The effect of different forcings on the recent (2000s) anomalies in the salinity

minimum are separated by subtracting hierarchically a forced simulation from another

simulation without that forcing. Salinity minimum changes in the UVic model (Figures

11b–d) are heterogeneous over the spatial domain (Figure 11). This feature agrees with

those features observed in SODA (Figure 6).

Adding SAM as a forcing mechanism (Figure 11b) produces mostly positive salinity

anomalies in the South Atlantic, and some negative anomalies in the Indian Ocean sector,

predominantly within the mixed layer. Anomalies forced by SAM are mostly driven by a

strengthening and displacement of the westerlies southward.

Anomalies generated by a historical NAO-like pattern (Figure 11c) are much weaker

with respect to those generated with SAM or CO_2 forcings, and show mostly negative

salinity anomalies within the subtropical gyre. Forcing due to increased CO_2 concentration

in the 2000s (Figure 11d) produces a salinity increase in the subtropical South Atlantic, and negative anomalies in shallower waters along the South Atlantic Current and ACC. The South Atlantic salinity response to CO_2 is similar but weaker than the response forced by SAM. This result is not what is expect considering the freshening that occurs in the Southern Ocean under global warming due to increased precipitation, as shown by the large negative anomalies south of 40°S. The analysis of zonal averaged salinity anomalies along isopycnals, remapped onto depth levels (Figure 12b), show that the freshening and warming in the Southern Ocean produce positive salinity anomalies on isopycnals, and this signal is spread northward along the salinity minimum surface. Slightly above the salinity minimum, there is freshening on isopycnals, which is consistent with previous works [*Curry et al.*, 2003; *Durack and Wijffels*, 2010; *Bindoff and Coauthors*, 2007]. Both salinification along isopycnals in the Southern Ocean and in the core of the AAIW, as well as the freshening above the core of the AAIW are consistent with the shoaling of the isopycnals and increased stratification driven by surface warming, in agreement with [*Schmidtko and Johnson*, 2012]. The SAM effect on salinity on isopycnals is somewhat opposite to CO_2, with salinification on the upper part of the AAIW, and freshening below the salinity minimum, and south of 50°S.

The time series of salinity and temperature at the location of the salinity minimum at 30°S/25°W for the UVic model are shown in Figure 13. The CONTROL simulation, without transient forcing (red curve), shows a salinity of ~ 34.57 and temperature of ~ 4.39 °C at the salinity minimum depth from 1870 to 2009. Salinity changes, relative to the CONTROL simulation, that are driven by wind changes in response to the SAM atmospheric pressure forcing (green curve in Figure 13a) are negative from 1870 to 1950

in the model. Changes in the SAM phase after the 1960s strengthen and displace the westerlies southward, driving positive salinity anomalies that are modulated by decadal variability. In 2008, the salinity is 0.015 above the pre-industrial level. When a NAO-like forcing is considered in addition to the SAM forcing (blue curve in Figure 13), additional changes are minor, and the trends due to wind variability do not differ from the SAM-only experiment. Finally, when CO_2 forcing is added on the top of SAM and NAO forcings (turquoise curve in Figure 13), there is an increase in the positive trend in the salinity minimum after 1950 in comparison to the SAM-only experiment. This trend driven by the CO_2, load in the atmosphere is strongly linear. The 2008 salinity anomaly relative to the pre-industrial values is 0.025 psu. Therefore, the CO_2 indirect forcing though wind changes is responsible for 50% of the simulated AAIW salinity anomalies due to SAM in the 2000s.

Although secondary in driving historical salinity anomalies in the AAIW, CO_2 forcing is the main contributor for the increase in temperature anomalies at the depth of the salinity minimum (Figure 13b). While SAM-like forcing accounts for 0.1°C relative to the CONTROL run, adding the CO_2 forcing has a direct effect to increase the temperature anomalies to 0.3°C, a contribution of 2/3 of the recent warming of the AAIW, while SAM accounts for just 1/3. The NAO-like forcing is again a minor contribution to the AAIW variability in the South Atlantic.

4. Discussion and Conclusions

By investigating the decadal changes in the minimum salinity layer for the subtropical South Atlantic, we have established the relationship between density changes with large scale climate trends. We used outputs from a reanalysis product, SODA 2.2.6, to verify the

changes in the salinity minimum from 1960s. The changes in more recent years (starting in 1992) are compared to another reanalysis, ECCO2. The two products produce different climatologies of salinity minimum in the 2000s, and ECCO2 shows less bias towards observations, since it assimilates both surface and profiles data. In SODA, the AAIW core reaches depths of 1200 m, in comparison to 800m for Argo observations and ECCO2. Therefore, SODA shows stronger isopycnal slopes around the outcropping region of the AAIW in the South Atlantic (45°–50°S), and the salinity minimum signature in depth spreads unsullied further north than observations and ECCO2. Both processes suggest weak isopycnal mixing in SODA. The slope of the isopycnals in the Southern Ocean is mostly set by the westerly winds strength, and partly compensated by an opposing eddy-induced circulation, which is mostly directed along isopycnals [e.g., *Marshall and Radko*, 2003; *Olbers and Visbeck*, 2005; *Meredith et. al*, 2012]. This feature is generally parameterized in climate models using the *Gent and McWilliams* [1990] scheme. Some of the mismatches in the modeled AAIW climatologies may also result from different vertical resolutions. The vertical grid spacing in SODA at the depth of about 1000m is approximately 250m, whereas in ECCO2 it is ∼100m. These limitations can potentially be overcome with improved parameterizations and calibrated mixing parameter values [*Goes et al.*, 2010; *Gent et al.*, 2011].

Even though the climatology of the AAIW differ, the two reanalysis agree well in terms of the variability in the last two decades. Significant trends are observed in SODA and ECCO2 since the late 1990s in salinity, temperature and density at intermediate levels. We found a latitudinal dependence on the contribution of temperature and salinity to density changes that would ultimately drive the meridional water displacement in the

ocean. South of 30°S, and within the subtropical gyre, there is strong compensation between salinity and temperature, which may drive larger trends in those fields because of the dynamical influence of salinity. North of 30°S, salinity and temperature changes are positively correlated, and temperature dominates the density changes.

In SODA, we determined two main dynamic factors for the salinity increase in the South Atlantic salinity minimum region: i) the expansion and spin up of the subtropical gyre, driven by enhanced wind stress curl and a shift southward, increases mixing of high salinity Agulhas leakage waters into the South Atlantic; and ii) the strengthening of the westerlies forces an increase in the Agulhas leakage, and, therefore, the input of high salinity waters at intermediate depths into the South Atlantic.

Different dynamic mechanisms are also present at different latitudes which determine the spread of the high salinity waters from the southeast boundary into the Atlantic. Our results show that the strengthening of the westerlies are positively correlated with the salinity minimum anomalies in most part the basin. At 30°S, the salinity anomalies generated by increased westerlies in the southeastern Atlantic follow a path defined by the Benguela Current and the Benguela Current Extension, in which changes in salinity at this latitude are highly driven by ocean adjustment through a second mode Rossby wave mechanism. This result is in agreement with previous studies [e.g., *McCarthy et al.*, 2012; *Durgadoo et al.*, 2013], and in both SODA and ECCO2 reanalysis. Therefore, the reported present-day leakage increase could reflect an unadjusted oceanic response mainly to the strengthening westerlies over the last few decades.

At 35°S, there is a discontinuity in the propagation pattern at approximately 15°W, and the propagation speeds of the westward salinity anomalies, revealed by the method

applied here, are much slower than what linear wave theory predicts. Previous studies have shown that bathymetric features, such as the Mid-Atlantic Ridge can discontinue the propagation of Rossby waves [*Vianna and Menezes*, 2013]. This does not seem to be the case here, since at 35°S the steepest part of the Ridge is located at approximately 0°W. Instead, a PV front at that latitude prevents the spread of the anomalies westward reducing the mixing of high salinity anomalies from the Agulhas leakage region, similar to the effect described in [*Beal et al.*, 2006]. The lags of the maximum correlation show that salinity anomalies take up to 17 years to cross basin since they are forced in the eastern side. The southwestern side of the basin, near the Brazil-Malvinas Confluence, show negative and not statistically significant correlations with salinity minimum anomalies in the southwestern part of the basin. Although the results can have biases with respect to the circulation patterns presented by SODA at intermediate levels, these results corroborate to our above mentioned results showing that at the latitudes where salinity anomalies cannot freely propagate westward, other processes may be determine the regional variability of salinity. In fact, as described in *Schmidtko and Johnson* [2012], the southwestern region of the South Atlantic shows a negative and not significant salinity trend at intermediate levels, in opposition with the positive salinity decadal trend in most of the South Atlantic.

The sensitivity studies with the UVic2.9 model indicate that the SAM is the predominant forcing of salinity changes in the sub-surface South Atlantic when compared to the NAO and CO_2 forcing. The positive trend in SAM, largely attributed to stratospheric ozone depletion [*Thompson et al.*, 2011], is associated with cooling at high southern latitudes and strengthening of the latitudinal temperature gradient, leading to stronger sub-tropical and westerly winds, and a southward displacement of the westerlies [*Hall and*

527 *Visbeck*, 2002; *Silvestri and Vera*, 2003; *Lefebvre et al.*, 2004; *Sen Gupta and England*,

528 2006; *Gillett et al.*, 2006; *Toggweiler*, 2009; *Thompson et al.*, 2011]. The strengthening and

529 southward displacement of the westerlies increase the Agulhas leakage [*Durgadoo et al.*,

530 2013], in a mechanism that must be unrelated to the model resolution. NAO variability,

531 which largely affects the water masses properties in the the North Atlantic [*Arbic and*

532 *Owens*, 2001], and the water mass formation of the Labrador Sea and Greenland Sea

533 water, does not seem to affect the spread of the salinity minimum in the South Atlantic.

534 This result can have implications for paleoclimate studies, which relate the water mass

535 formation in both hemispheres as a potentially coupled system [*Wainer et al.*, 2012].

536   Warming due to CO_2 loading increases precipitation relatively to evaporation in the

537 Southern Ocean [*Curry et al.*, 2003; *Held and Soden*, 2006; *Durack and Wijffels*, 2010;

538 *Helm et al.*, 2010], producing a surface freshening of the ocean [*Boyer et al.*, 2005; *Böning*

539 *et al.*, 2008]. Although this region encompasses the formation regions of the AAIW, our

540 experiments show a salinity increase along isopycnal in the Southern Ocean and in the

541 salinity minimum surface due to CO_2. Our results suggest that the strong warming and

542 freshening that happens south of 45°S decrease the density and shoals the isopycnals, in

543 agreement with [*Schmidtko and Johnson*, 2012].

544   *Bindoff and McDougall* [1994] analyze salinity and temperature changes in isopycnals

545 as pure heating, pure freshening and heave. More recent studies call attention to the

546 lateral advection of these properties along isopycnals, and therefore, circulation changes

547 would be a source of salinity changes on isopycnals [*Durack and Wijffels*, 2010; *Schmidtko*

548 *and Johnson*, 2012]. Here we confirm the role of lateral advection in increasing leakage of

549 salty Agulhas waters at intermediate levels, driven by the large-scale wind variability in the

region. Observational studies using satellite altimetry [e.g., *Backeberg et al.*, 2012], indeed suggest that the Agulhas leakage may have increased from 1993 to 2009, conrming previous modelling studies [e.g., *Biastoch et al.*, 2008], and the increased Agulhas leakage may have large-scale impacts by compensating a potential deceleration of meridional overturning circulation.

Appendix A: The climate model of intermediate complexity

In the present work we use the latest version of the University of Victoria Earth System Model (UVic 2.9). The ocean component of UVic 2.9 [*Weaver et al.*, 2001] is MOM2 [*Pacanowski*, 1995] with a 1.8° x 3.6° resolution in the horizontal and 19 depth levels. Diapycnal diffusivity is parameterized as $K_v = K_{tidal} + K_{bg}$, which consists of the mixing due to local dissipation of tidal energy (K_{tidal}) [*Laurent et al.*, 2002; *Simmons et al.*, 2004] plus a background diffusivity $K_{bg} = 0.3$ cm^2 s^{-1}. The atmospheric component is a one-layer atmospheric energy-moisture balance model, which does not apply flux correction and is forced by prescribed winds from the NCEP/NCAR climatology. Also included in the model are a thermodynamic sea ice component, a terrestrial vegetation (TRIFFID), and an oceanic biogeochemistry based on the ecosystem model of [*Schmittner*, 2005]. The model is spun up for 3000 years, and then four experiments are performed (Table 1). First, the CONTROL experiment is a non-transient experiment forced with atmospheric forcings from the 1800 levels. The second to fourth experiments use, in addition to the NCEP/NCAR wind stress climatology, wind stress anomalies calculated from the first empirical mode (EOF1) of sea level pressure (SLP) anomalies in the northern and southern hemispheres (Figure 14). These modes are a good approximation of the North Atlantic Oscillation (NAO), in which the positive phase is characterized by low SLP anomalies

over Iceland and high SLP anomalies over the Azores, and the Southern Annular Mode (SAM), which is characterized by low SLP anomalies over Antarctica, respectively. More specifically, the second experiment uses the SAM EOF forcing only, the third experiment uses the NAO EOF forcing only, and the fourth experiment uses both the SAM and the NAO forcings plus historical global CO_2 emissions, under which the atmospheric CO_2 concentration levels reach 384 ppmV in 2009. The hemispheric SLP modes are calculated from the *Compo et al.* [2006] dataset and start in the year 1871. When the SLP anomalies related to the hemispheric modes of variability are added to the model, the associated wind stress anomalies are calculated using a frictional geostrophic approximation [*Weaver et al.*, 2001]. In addition to the SLP anomalies added to the the climatological wind field, wind stress anomalies can be further produced as a linear dynamic coupling to SAT anomalies [*Weaver et al.*, 2001]. In UVic , the wind stress is converted to wind speed for the calculation of the latent and sensible heat fluxes from the ocean [*Fanning and Weaver*, 1998]. All experiments are run from 1800–2008, keeping the other atmospheric forcings (e.g., sulphate and volcanic aerosols) at the 1800 level.

References

Arbic, B. K., and W. B Owens (2001), Climatic warming of Atlantic Intermediate waters*, *J. Climate*, *14*, 4091–4108.

Backeberg, B. C., P. Penven, M. Rouault (2012), Impact of intensified Indian Ocean winds on mesoscale variability in the Agulhas system, *Nature Clim. Change*, *2*, 8, 608–612.

Barron, C. N., A. B. Kara, and G. A. Jacobs (2009), Objective estimates of westward Rossby wave and eddy propagation from sea surface height analyses, *J. Geophys. Res.*, *114*, C03,013.

Beal, L. M., Chereskin, T. K., Y. D. Lenn, and S. Elipot (2006), The sources and mixing characteristics of the Agulhas Current, *J. Phys. Oceanog.*, *36*, 2060–2074.

Biastoch, A., C. W. Böning, and J. R. E. Lutjeharms (2008), Agulhas leakage dynamics affects decadal variability in Atlantic overturning circulation, *Nature*, *456*, 489–492.

Bindoff, N. L., and T. J. McDougall (1994), Diagnosing climate change and ocean ventilation using hydrographic data, *J. Phys. Oceanogr.*, *24*, 1137–1152.

Bindoff, N. L., and Coauthors (2007), Observations: Oceanic climate change and sea level. *Climate Change 2007: The Physical Science Basis*, S. Solomon et al., Eds., Cambridge University Press, 385–432.

Böning, C. W., A. Dispert, S. M. Visbeck, R. Rintoul, and F. U. Schwarzkopf (2008), The response of the Antarctic Circumpolar Current to recent climate change, *Nature Geosci.*, *1*, 864–869.

Boyer, T., S. Levitus, J. Antonov, R. Locarnini, and H. Garcia (2005), Linear trends in salinity for the world ocean, 1955–1998, *Geophys. Res. Lett.*, *32*(1), 1–4.

Carton, J., and B. Giese (2008), A reanalysis of ocean climate using simple ocean data assimilation (SODA), *Mon. Weath. Rev.*, *136*(8), 2999–3017.

Challenor, P. G., P. Cipollini, and D. Cromwell (2001), Use of the 3D Radon transform to examine the properties of oceanic Rossby waves, *J. Atmos. Oceanic Technol.*, *18*, 1558–1566.

Compo, G., J. Whitaker, and P. Sardeshmukh (2006), Feasibility of a 100-year reanalysis using only surface pressure data, *Bull. Amer. Meteor. Soc.*, *87*, 175–190.

Compo, G., J. Whitaker, P. Sardeshmukh, N. Matsui, R. Allan, X. Yin, B. Gleason, R. Vose, G. Rutledge, P. Bessemoulin, et al. (2011), The twentieth century reanalysis project, *Quart. Jour. Royal Met. Soc.*, *137*(654), 1–28.

Curry, R., B. Dickson, I. Yashayaev (2003), A change in the freshwater balance of the Atlantic ocean over the past four decades, *Nature*, *426*(6968), 826–829.

Domingues, C. M., J. A. Church, N. J. White, P. J. Gleckler, S. E. Wijffels, P. M. Barker, and J. R. Dunn (2008), Improved estimates of upper-ocean warming and multi-decadal sea-level rise, *Nature*, *453*(7198), 1090–1093.

Durack, P., and S. Wijffels (2010), Fifty-year trends in global ocean salinities and their relationship to broad-scale warming, *J. Climate*, *23*(16), 4342–4362.

Durgadoo, J. V., B. R. Loveday, C. J. C. Reason, P. Penven, and A. Biastoch (2013), Agulhas leakage predominantly responds to the Southern Hemisphere westerlies, *J. Phys. Oceanogr.*, *43*, 2113–2131.

Fanning, A. F., and A. J. Weaver (1998), Thermohaline variability: The effects of horizontal resolution and diffusion, *J. Climate*, *11*(4), 709–715.

Garabato, A. C. N., L. Jullion, D. P. Stevens, K. J. Heywood, and B. A. King (2009), Variability of Subantarctic Mode Water and Antarctic Intermediate Water in the Drake passage during the late-twentieth and early-twenty-first centuries, *J. Climate*, *22*(13), 3661–3688.

Gent, P. R., and J. C. McWilliams (1990), Isopycnal mixing in ocean circulation models, *J. Phys. Oceanogr.*, *20*, 150–155.

Gent, P. R., and Coauthors (2011), The Community Climate System Model version 4, *J. Climate*, *24*, 4973–4991.

Gille, S. T. (2002), Warming of the Southern Ocean since the 1950s, *Science*, *295*, 1275–1277.

Gille, S. (2008), Decadal-scale temperature trends in the Southern Hemisphere ocean, *J. Climate*, *21*, 4749–4765.

Gillett, N., T. Kell, and P. Jones (2006), Regional climate impacts of the Southern Annular Mode, *Geophys. Res. Lett.*, *33*(23).

Goes, M., I. Wainer, P. R. Gent, and F. O. Bryan (2008), Changes in subduction in the South Atlantic Ocean during the 21st century in the CCSM3, *Geophys. Res. Lett.*, *35*, 6701–+.

Goes, M., N. M. Urban, R. Tonkonojenkov, M. Haran, A. Schmittner, and K. Keller (2010), What is the skill of ocean tracers in reducing uncertainties about ocean diapycnal mixing and projections of the Atlantic Meridional Overturning Circulation?, *J. Geophys. Res.*, *115*, C12006.

Goni, G. J. and Wainer, I. (2001), Investigation of the Brazil Current front variability from altimeter data, *J. Geophys. Res.*, *106*(C12), 31117–31128.

Goni, G. J., F. Bringas, and P. N. DiNezio (2011), Observed low frequency variability of the Brazil Current front, *J. Geophys. Res. – Oceans, 116*(C10037).

Gordon, A. L., R. F. Weiss, W. M. Smethie Jr., and M. J. Warner (1992), Thermocline and intermediate water communication between the South Atlantic and Indian oceans, *J. Geophys. Res., 97*(C5), 7223–7240.

Grodsky, S., J. Carton, and F. Bingham (2006), Low frequency variation of sea surface salinity in the tropical Atlantic, *Geophys. Res. Lett., 33*(14), L14,604.

Hall, A., and M. Visbeck (2002), Synchronous variability in the Southern Hemisphere atmosphere, sea ice, and ocean resulting from the annular mode*, *J. Climate, 15*(21), 3043–3057.

Held, I. M., and B. J. Soden (2006), Robust responses of the hydrological cycle to global warming, *J. Climate, 19*, 5686–5699.

Helm, K. P.,N. L. Bindoff, andJ. A. Church (2010), Changes in the global hydrological-cycle inferred from ocean salinity,*Geophys. Res. Lett., 37*, L18701.

Jackett, D. R., and T. J. McDougall (1997), A neutral density variable for the world's oceans, *J. Phys. Oceanogr., 27*, 237–263.

Laurent, L. S., H. Simmons, and S. Jayne (2002), Estimating tidally driven mixing in the deep ocean, *Geophys. Res. Lett., 29*(23), 2106.

Lefebvre, W., H. Goosse, R. Timmermann, and T. Fichefet (2004), Influence of the Southern Annular Mode on the sea ice–ocean system, *J. Geophys. Res.: Oceans, 109*(C9).

Levinson, D. H., and J. H. Lawrimore (2008), State of the climate in 2007, *Bull. Amer. Meteor. Soc., 89*, S1–S179.

Levitus, S., J. Antonov, T. Boyer, and C. Stephens (2000), Warming of the world ocean, *Science*, *287*, 2225–2229.

Levitus, S., J. I. Antonov, and T. P. Boyer (2005), Warming of the world ocean, 1955-2003, *Geophys. Res. Lett.*, *32*, L02,604.

Levitus, S., J. Antonov, T. Boyer, R. Locarnini, H. Garcia, and A. Mishonov (2009), Global ocean heat content 1955–2008 in light of recently revealed instrumentation problems, *Geophys. Res. Lett.*, *36*(7).

Lozier, M. S., V. Roussenov, M. S. C. Reed, and R. G. Williams (2010), Opposing decadal changes for the North Atlantic meridional overturning circulation. *Nature Geosc.*, *3*, 728–734.

Lumpkin, R., and S. Garzoli (2011), Interannual to decadal changes in the western South Atlantic's surface circulation, *J. Geophys. Res.*, *116*, C01014.

Lyman, J. M., S. A. Good, V. V. Gouretski, M. Ishii, G. C. Johnson, M. D. Palmer, D. M. Smith, and J. K. Willis (2010), Robust warming of the global upper ocean, *Nature*, *465*(7296), 334–337.

Marshall, J., A. Adcroft, C. Hill, L. Perelman, and C. Heisey (1997), A finite-volume, incompressible Navier Stokes model for studies of the ocean on parallel computers, *J. Geophys. Res.*, *102*(C3), 5753–5766.

Marshall, J., and T. Radko (2003), Residual-mean Solutions for the Antarctic Circumpolar Current and its associated overturning circulation, *J. Phys. Ocean.*, *33*, 2341–2354.

McCarthy, G., E. McDonagh, and B. King (2011), Decadal variability of thermocline and intermediate waters at 24°S in the South Atlantic, *J. Phys. Oceanogr.*, *41*, 157–165.

McCarthy, G. D., B. A. King, P. Cipollini, E. L. McDonagh, J. R. Blundell, and A. Bi-
astoch (2012), On the sub-decadal variability of South Atlantic Antarctic Intermediate
Water, *Geophys. Res. Lett*, *39*, L10,605.

McCartney, M. S. (1977), Subantarctic Mode Water. *A Voyage of Discovery*, M. V. Angel,
Ed., Pergamon, 103–119.

Menemenlis, D., I. Fukumori, and T. Lee (2005), Using Green's functions to calibrate an
ocean general circulation model. *Mon. Weather Rev.*, *133*, 1224–1240.

Menemenlis, D., J. Campin, P. Heimbach, C. Hill, T. Lee, A. Nguyen, M. Schodlok, and
H. Zhang (2008), ECCO2: High resolution global ocean and sea ice data synthesis.
Mercator Oce. Quart. Newsl., *31*, 13–21.

Meredith, M. E., A. C. Naveira Garabato, A. McC. Hogg, and R. Farneti (2012), Sensi-
tivity of the overturning circulation in the Southern Ocean to decadal changes in wind
forcing, *J. Climate*, *25*, 99–110.

Olbers, D., and M. Visbeck (2005), A model of the zonally averaged stratification and
overturning in the Southern Ocean, *J. Phys. Oceanogr.*, 1190–1205.

Onogi, K., J. Tsutsui, H. Koide, M. Sakamoto, S. Kobayashi, H. Hatsushika, T. Mat-
sumoto, N. Yamazaki, H. Kamahori, K. Takahashi, S. Kadokura, K. Wada, K. Kato, R.
Oyama, T. Ose, N. Mannoji, and R. Taira (2007), The JRA-25 Reanalysis, *J. Meteor.
Soc. Japan*, *85*, 369–432.

Pacanowski, R. (1995), MOM 2 documentation user's guide and reference manual, GFDL
Ocean Group Technical Report No.3, *Fluid Dyn. Lab. NOAA, Princeton, NJ.*

Peeters, F. J. C., R. Acheson, G.-J. A. Brummer, W. P. M. de Ruijter, G. M. Ganssen,
R. R. Schneider, E. Ufkes, and D. Kroon (2004), Vigorous exchange between Indian

727 and Atlantic Ocean at the end of the last five glacial periods, *Nature*, *430*, 661–665.

728 Pierce, D. W., P. J. Gleckler, T. P. Barnett, B. D. Santer, and P. J. Durack (2012), The

729 fingerprint of human-induced changes in the oceans salinity and temperature fields,

730 *Geophys. Res. Lett.*, *39*, L21,704.

731 Polito, P. S., and W. T. Liu (2003), Global characterization of Rossby waves at several

732 spectral bands, *J. Geophys. Res.*, *108*.

733 Ray, S., and B. S. Giese (2012), Historical changes in El Niño and La Niña characteristics

734 in an ocean reanalysis, *J. Geophys. Res.*, *117*, C11,007.

735 Roemmich, D., and J. Gilson (2009), The 2004-2008 mean and annual cycle of temper-

736 ature, salinity, and steric height in the global ocean from the Argo program, *Progr.*

737 *Oceanogr.*, *82*, 81–100.

738 Roemmich, D., J. Gilson, R. Davis, P. Sutton, S. Wijffels, and S. Riser (2007), Decadal

739 spinup of the South Pacific subtropical gyre, *J. Phys. Oceanogr.*, *37*, 162–173.

740 Saenko, O. A., A. J. Weaver, and M. H. England (2003), A region of enhanced northward

741 Antarctic Intermediate Water transport in a coupled climate model, *J. Phys. Oceanogr.*,

742 *33*, 1528–1535.

743 Saenko, O. A., John C. Fyfe, and M. H. England (2005), On the response of the oceanic

744 wind-driven circulation to atmospheric CO2 increase, *Clim. Dyn.*, *25*, 415–426.

745 Schmid, C., G. Siedler, and W. Zenk (2000), Dynamics of Intermediate Water circulation

746 in the subtropical South Atlantic, *J. Phys. Oceanogr.*, *30*, 3191–3211.

747 Schmid, C., and S. L. Garzoli (2009), New observations of the spreading and variability

748 of the Antarctic Intermediate Water in the Atlantic, *J. Marine Res.*, *67*(6), 815–843.

Schmidtko, S., and G. Johnson (2012), Multidecadal warming and shoaling of Antarctic Intermediate Water*, *J. Climate*, *25*, 207–221.

Schmittner, A. (2005), Decline of the marine ecosystem caused by a reduction in the Atlantic overturning circulation, *Nature*, *434*(7033), 628–633.

Sen Gupta, A., and M. H. England (2006), Coupled ocean-atmosphere-ice response to variations in the Southern Annular Mode, *J. Climate*, *19*(18), 4457–4486.

Silvestri, G. E., and C. S. Vera (2003), Antarctic oscillation signal on precipitation anomalies over southeastern South America, *Geophys. Res. Lett.*, *30*(21), 2115.

Simmons, H. L., S. R. Jayne, L. C. S. Laurent, and A. J. Weaver (2004), Tidally driven mixing in a numerical model of the ocean general circulation, *Ocean Modell.*, *6*(3), 245–263.

Smith, R., J. Dukowicz, and R. Malone (1992), Parallel ocean general circulation modeling, *Physica D: Nonlinear Phenomena*, *60*(1), 38–61.

Talley, L. D. (2002), *Salinity patterns*, 11 pp., Encyclopedia of Global Environmental Change, vol. 1, M. C. MacCracken and J. S. Perry, editors, John Wiley and Sons.

Thompson, D. W., S. Solomon, P. J. Kushner, M. H. England, K. M. Grise, and D. J. Karoly (2011), Signatures of the Antarctic ozone hole in Southern Hemisphere surface climate change, *Nature Geosc.*, *4*(11), 741–749.

Toggweiler, J. (2009), Shifting westerlies, *Science*, *323*(5920), 1434–1435.

Trenberth, K. E., and Coauthors (2007), *Observations: Surface and atmospheric climate change*, 235–336 pp., S. Solomon et al., Eds., Cambridge University Press.

Vianna, M. L., and V. V. Menezes (2013), Bidecadal sea level modes in the North and South Atlantic Oceans, *Geophys. Res. Lett.*, *40*, 5926–5931.

Wainer, I., Gent, P., and Goni, G. (2000), Annual cycle of the Brazil-Malvinas Conflu-
ence region in the National Center for Atmospheric Research climate system model, *J.
Geophys. Res.*, *105*(C11), 26167–26177.

Wainer, I., Goes, M., Brady, E., and Murphy, L. (2012), Changes in the Intermediate
Water mass formation rates in the global ocean for the Last Glacial Maximum, Mid-
Holocene and Pre-Industrial climates, *Paleoceanogr.*, *27*, PA3101.

Weaver, A. J., M. Eby, E. C. Wiebe, C. M. Bitz, P. B. Duffy, T. L. Ewen, A. F. Fanning,
M. M. Holland, A. MacFadyen, H. D. Matthews, et al. (2001), The UVic Earth system
climate model: Model description, climatology, and applications to past, present and
future climates, *Atmos.-Oc.*, *39*(4), 361–428.

Weijer, W., W. P. M. de Ruijter, A. Sterl, and S. S. Drijfhout (2002), Response of the
Atlantic overturning circulation to South Atlantic sources of buoyancy, *Global Planet.
Change*, *34*, 293–311.

You, Y. (2002), Quantitative estimate of Antarctic Intermediate Water contributions from
the Drake Passage and the southwest Indian Ocean to the South Atlantic, *J. Geophys.
Res.*, *107*, 3031.

Table 1. Summary of the climate model experiments.

Experiment	Wind Forcing	CO_2 Forcing
CONTROL	NCEP climatology	1800 level
SAM	NCEP clim plus SAM	1800 level
SAM + NAO	NCEP clim plus SAM plus NAO	1800 level
SAM + NAO + CO_2	NCEP clim plus SAM plus NAO	Transient to 384 ppmV in 2009
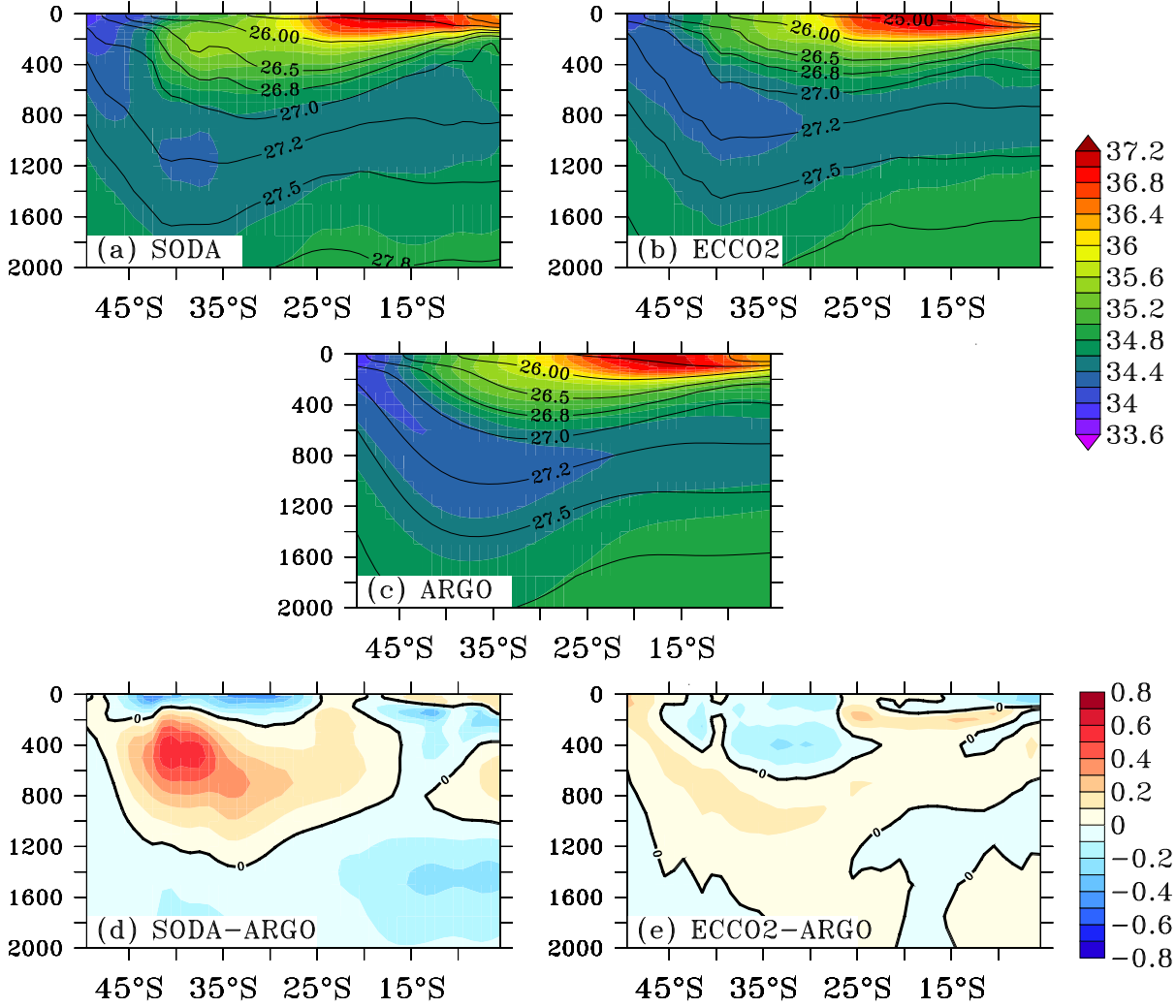
Figure 1. Meridional section of the climatological average (after 2004) of salinity at 25°W in the South Atlantic. Depth is in meters. Relevant potential density surfaces (σ_θ in kg/m³) are overlaid. Panel a) is for SODA, b) for ECCO2, c) for Argo climatology [*Roemmich and Gilson*, 2009], d) SODA - Argo and e) ECCO2 - Argo.
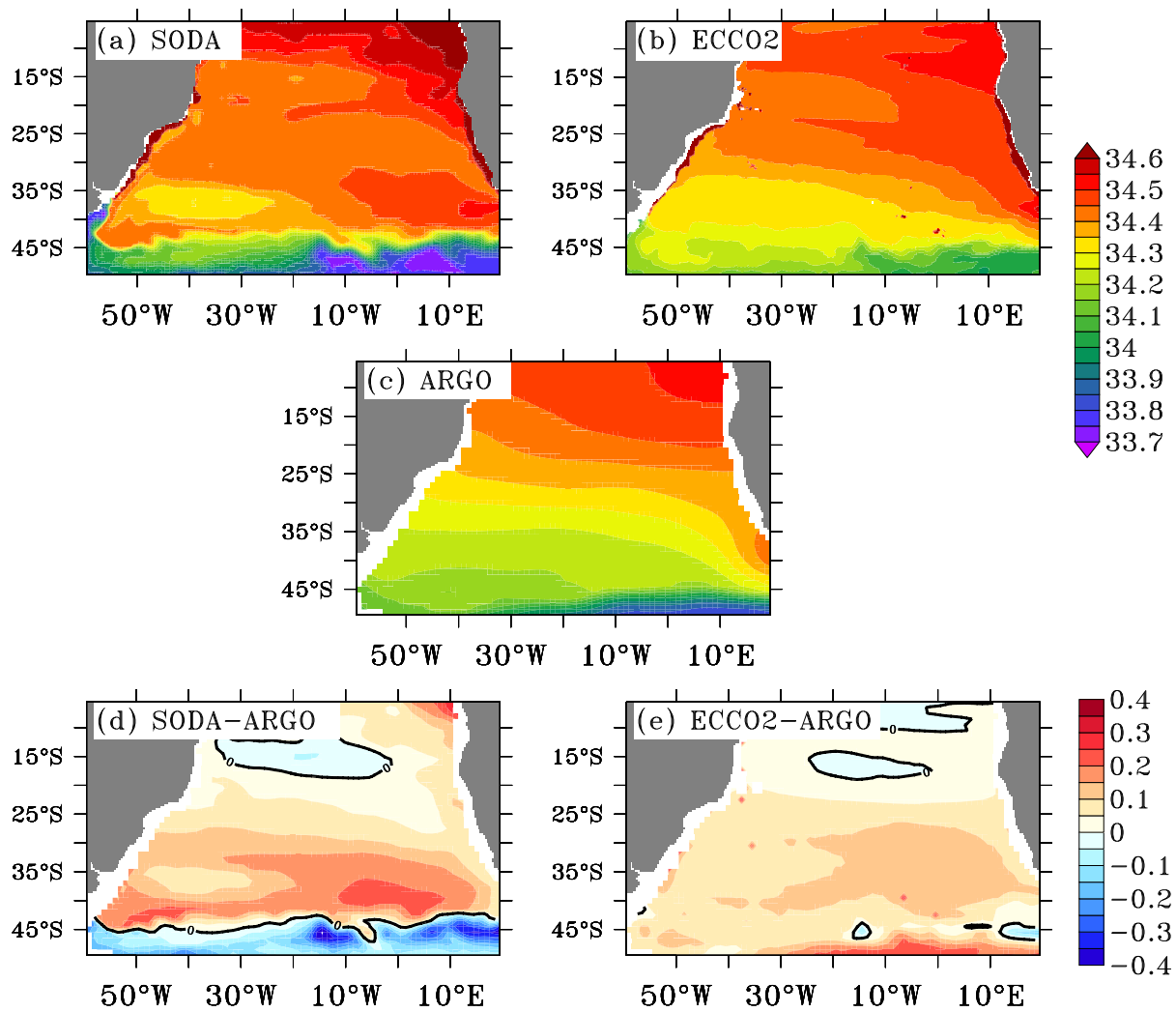
Figure 2. Maps of the climatological average (after 2004) of the salinity minimum surface in the South Atlantic. Panel a) is for SODA, b) for ECCO2, c) for Argo climatology [*Roemmich and Gilson*, 2009], d) SODA - Argo and e) ECCO2 - Argo.
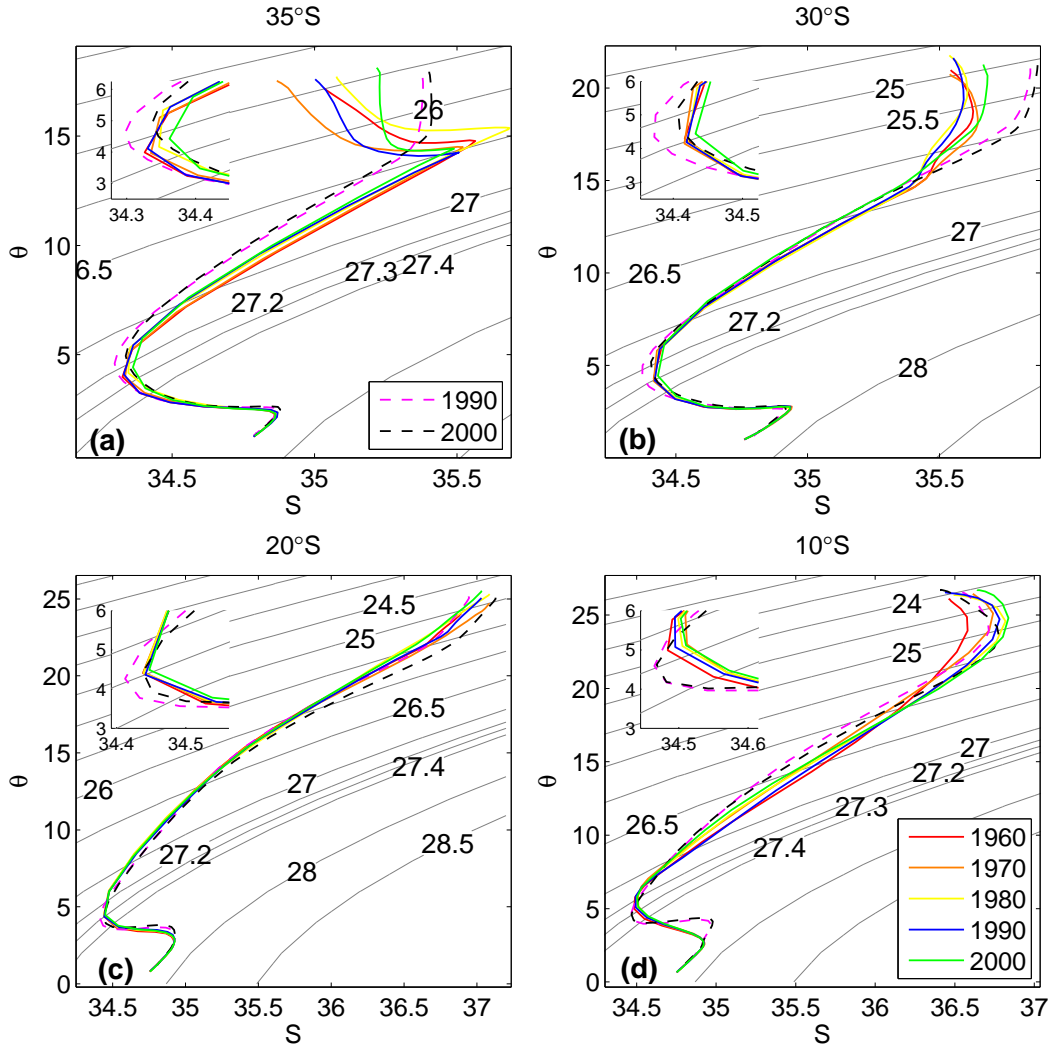
Figure 3. Θ/S diagram for the South Atlantic Ocean at 25°W for a) 35°S, b) 30°S, c) 20°S and d) 10°S. Solid colored lines represent SODA's decadal averages for the 1960s (red), 1970s (orange), 1980s (yellow), 1990s (green) and 2000s (blue). Dashed colored lines represent ECCO2's decadal averages for 1990s (magenta) and 2000s (black).
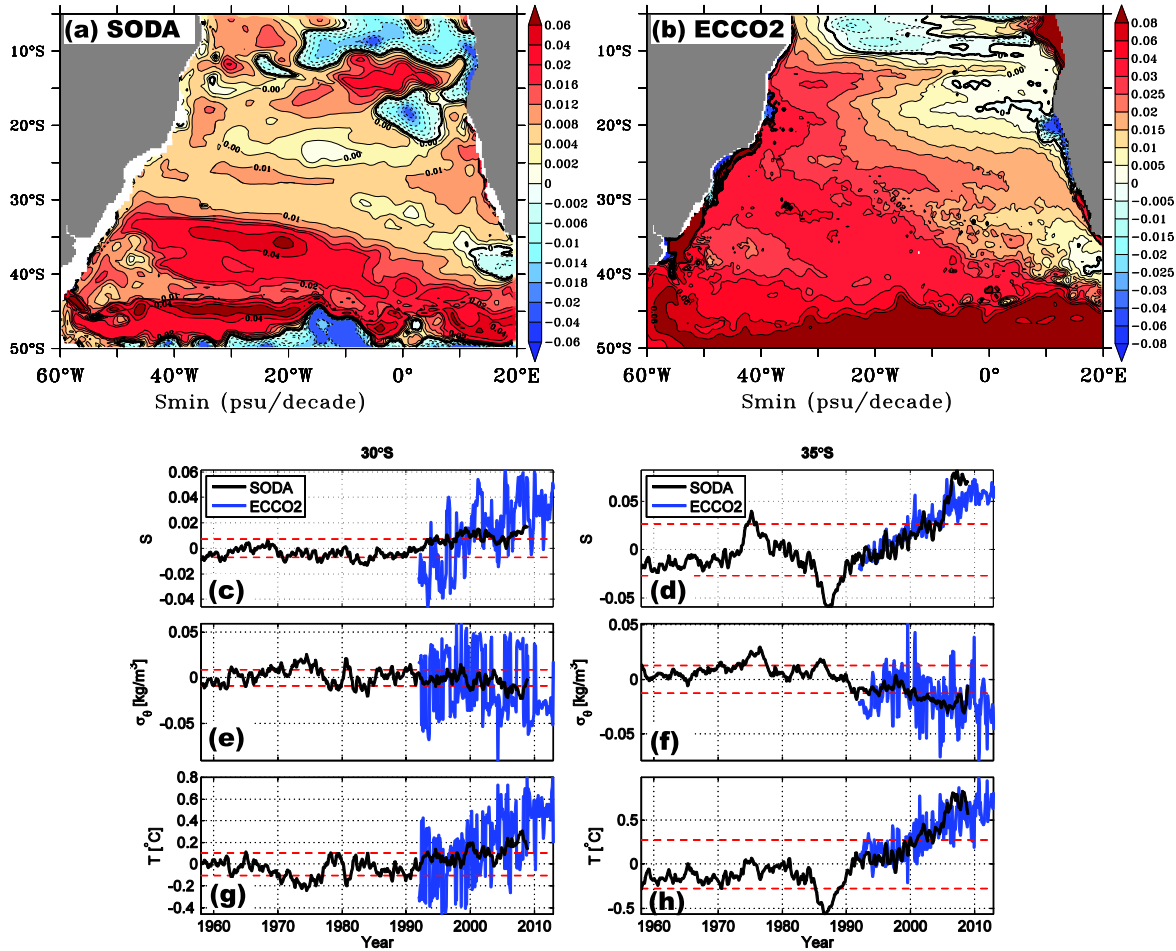
Figure 4. Salinity minimum trend between 1990's and 2000's (psu/decade) for (a) SODA and (b) ECCO2. Panels (c-h) are the time series of the salinity (c, d), sigma density (e,f), and temperature (g,h) anomalies with respect to SODA's 1960-2008 period at the location of the salinity minimum. Timeseries on the left column are for 25°W/30°S and on the right column for 25°W/35°S. Black timeseries is for SODA and blue is for ECCO2. The red dashed lines represent SODA's three standard deviation levels relative to each parameter.
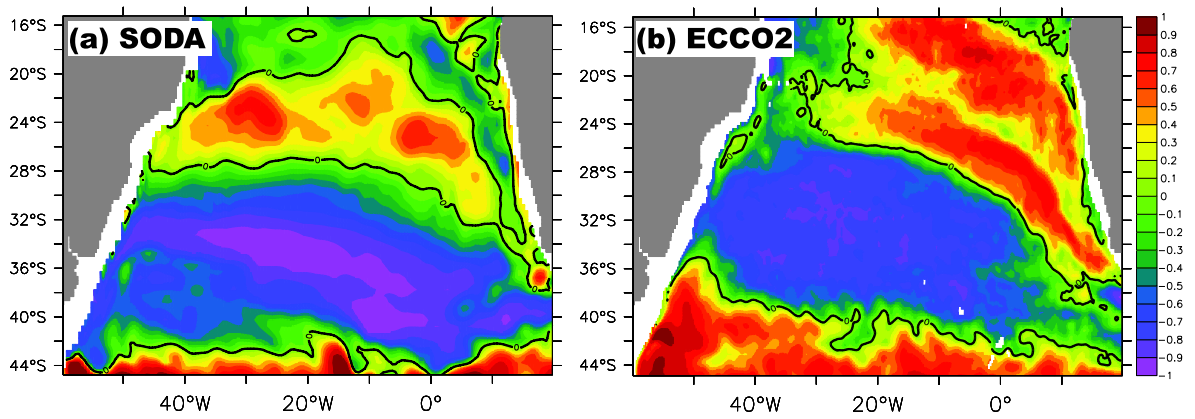
Figure 5. Correlation between the components of the sigma density, i.e., thermopycnal and halopycnal components, at approximately 1100 m depth for (a) SODA and (b) ECCO2. The components of sigma are calculated by keeping the other component as the climatological value.
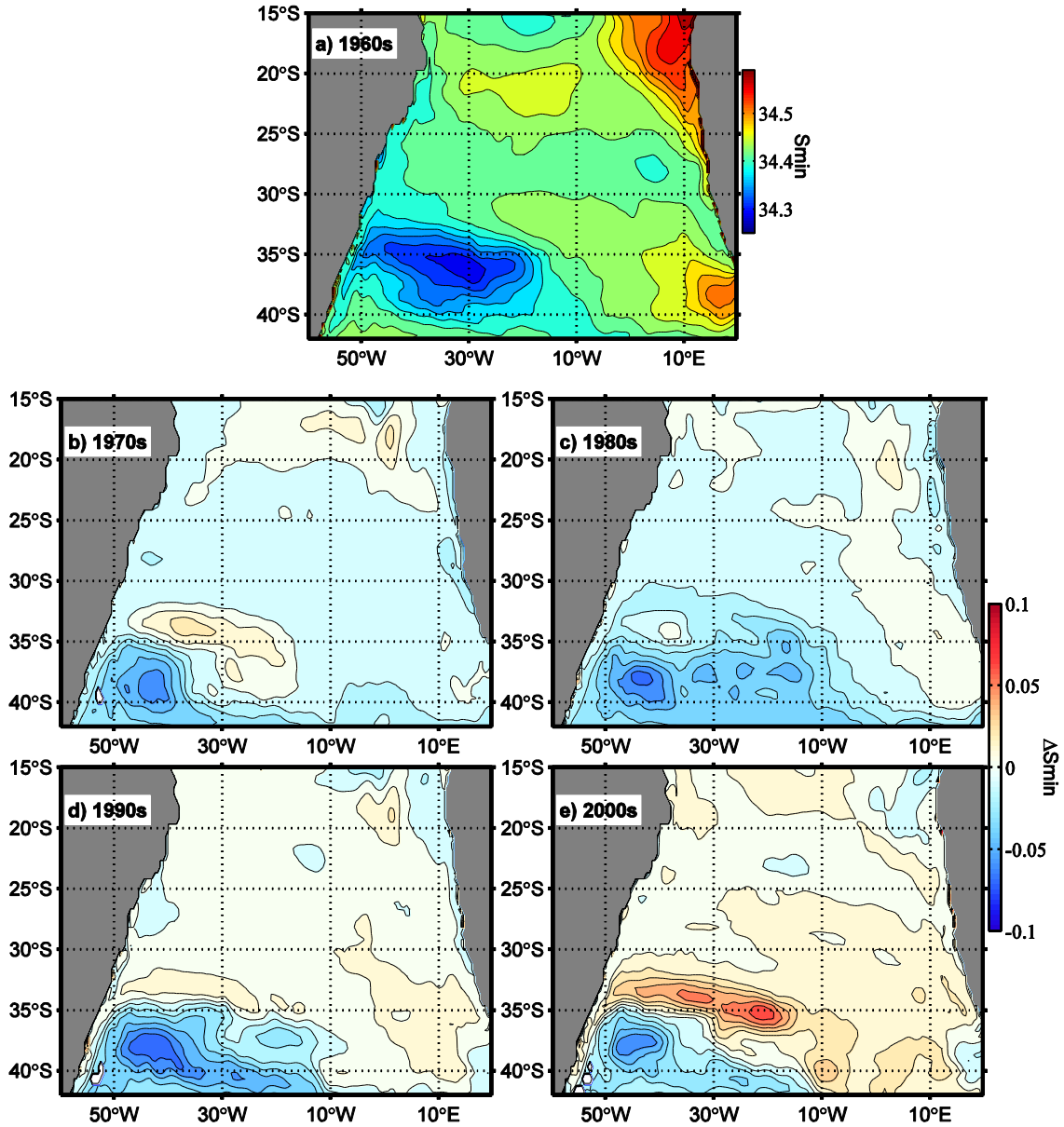
Figure 6. Salinity minimum within the layer defined by the $\gamma_n = 27.1$ and $\gamma_n = 27.6$ neutral surfaces for a) 1960s, and anomalies relative to 1960s for b) 1970s, c) 1980s, d) 1990s and e) 2000s.
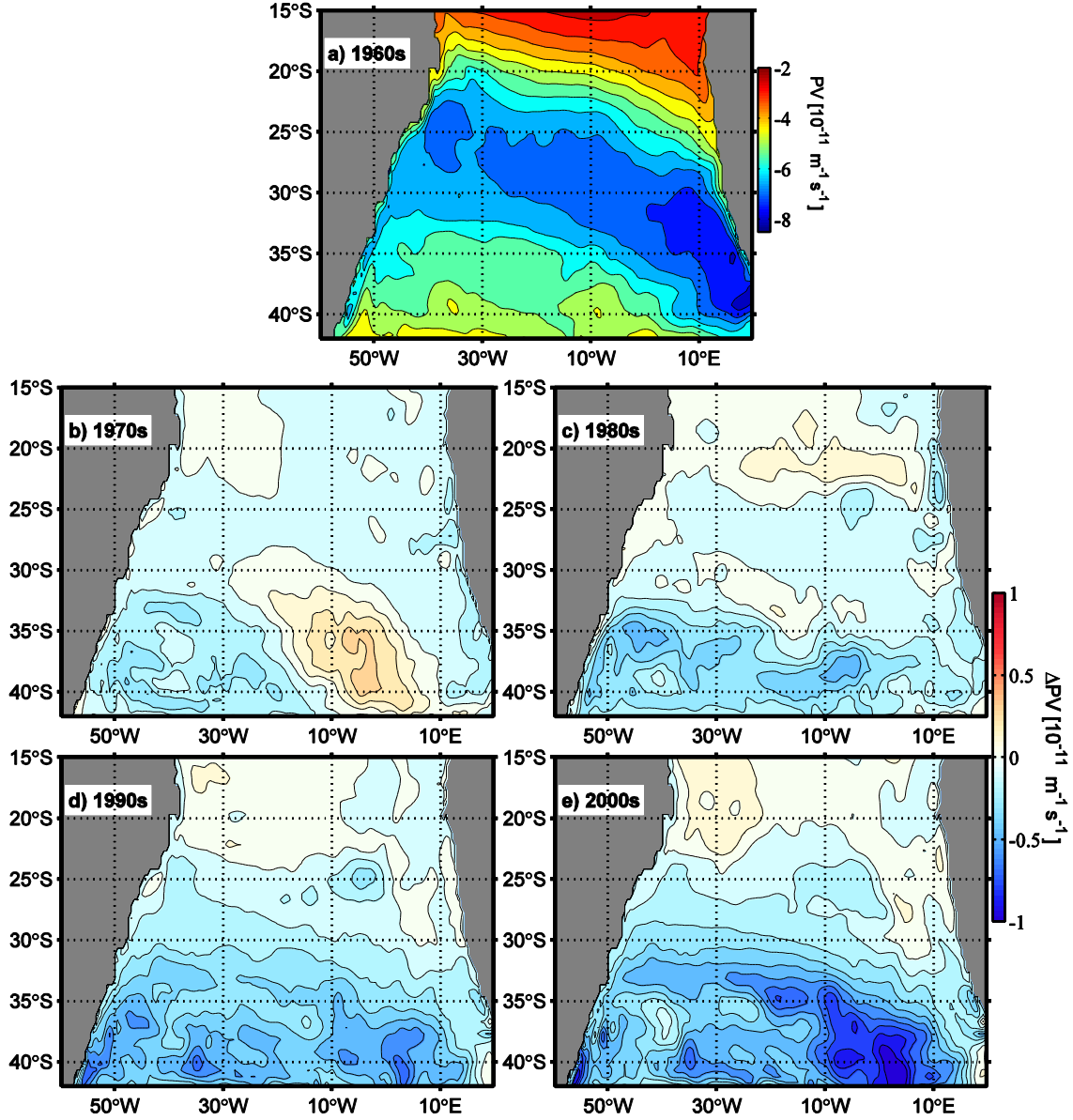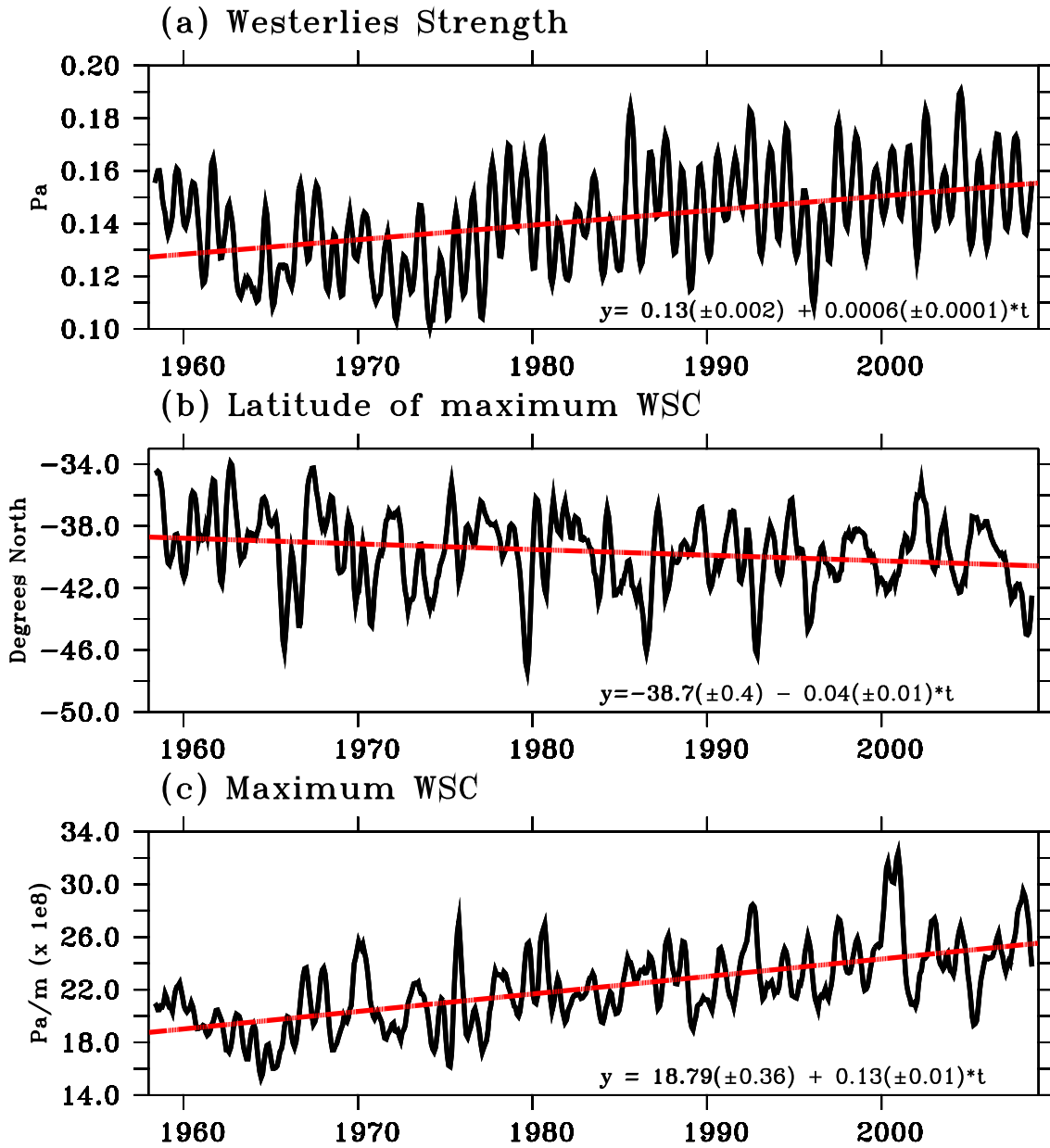
Figure 7. Ertel's potential vorticity calculated within the layer defined by the $\gamma = 27.1$ and $\gamma = 27.6$ neutral surfaces for a) 1960s, and anomalies relative to 1960s for b) 1970s, c) 1980s, d) 1990s and e) 2000s.

Figure 8. SODA wind stress indices for the eastern South Atlantic (0–20°E) of (a) westerlies strength (Pascal), (b) latitude of the maximum zonal average wind stress curl (degrees north), and (c) maximum zonal average wind stress curl (Pascal/meter×$1e^{-8}$).Linear regressions are overlaid in red, and the estimated regression parameters are displayed on the right bottom of each panel, with their 95% credibility interval in parenthesis and time (t) in years.
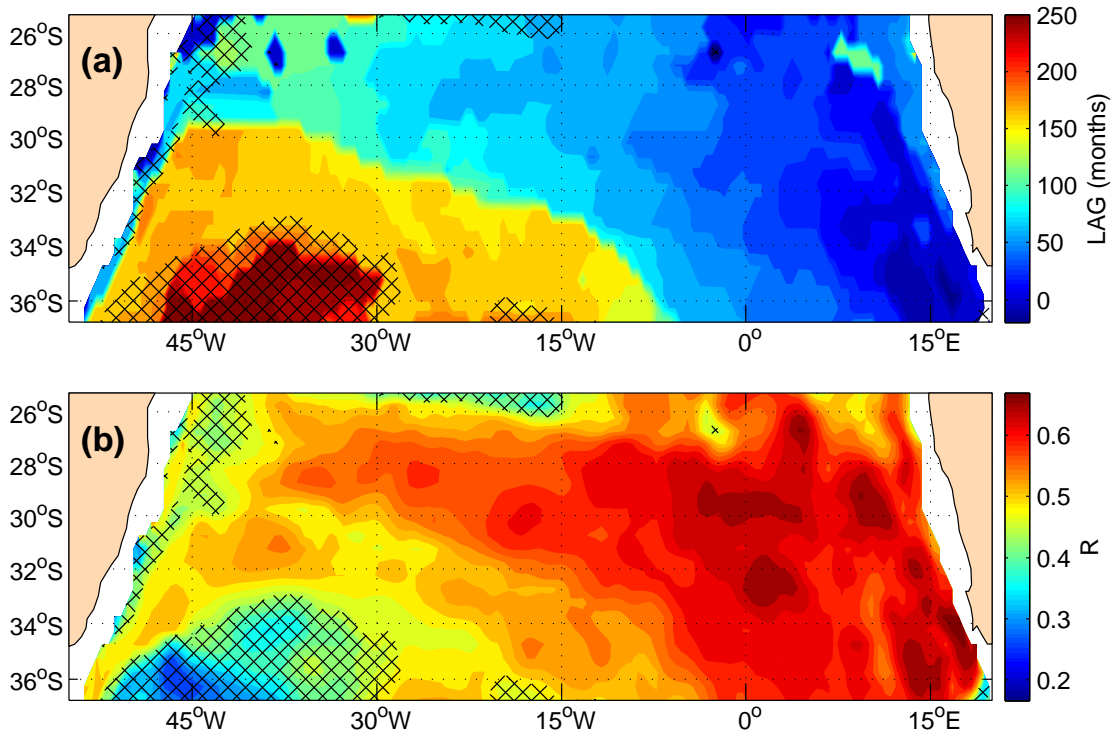
Figure 9. Maximum lagged correlation between the salinity at $\sigma_\theta = 27.2$ and a westerly wind strength index in the southeastern Atlantic, defined by the τ_x averaged between 35°S–65°S/0°E–20°E. (a) is the lag of the maximum correlation (months) and (b) is the maximum correlation. The crossed areas are where correlation values of the pre-whitened timeseries are not statistically significant.
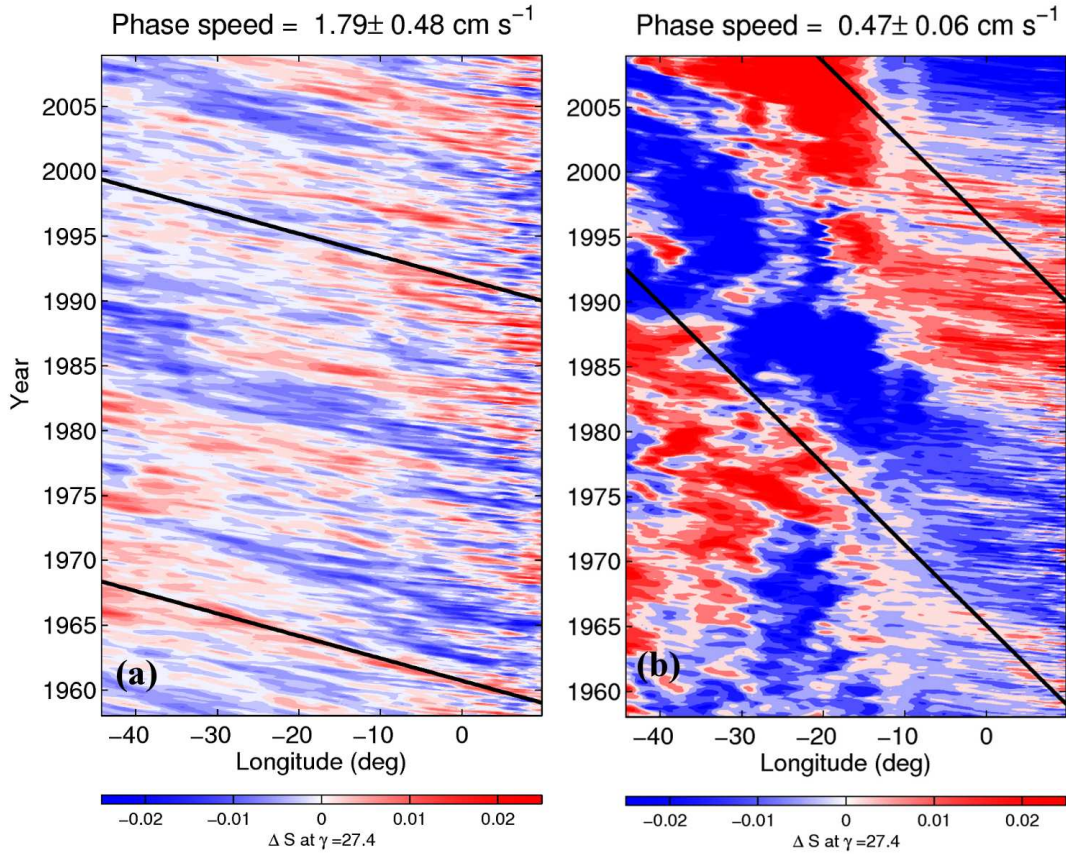
Figure 10. Time x Longitude diagram for the salinity anomalies projected onto the neutral density surface $\gamma_n = 27.4$, that defines the region of minimum salinity in the subtropical Atlantic at (a,c) 30°S and (b,d) 35°S. Panels (a,b) are for SODA and (c,d) are for ECCO2. Following *Barron et al.* [2009], the zonal average of the salinity anomalies is subtracted from the diagrams to highlight the propagating features. The phase speed calculated from the method of *Barron et al.* [2009] is shown on the top of each panel and its displacement is shown as a black line overlaid on the contours.
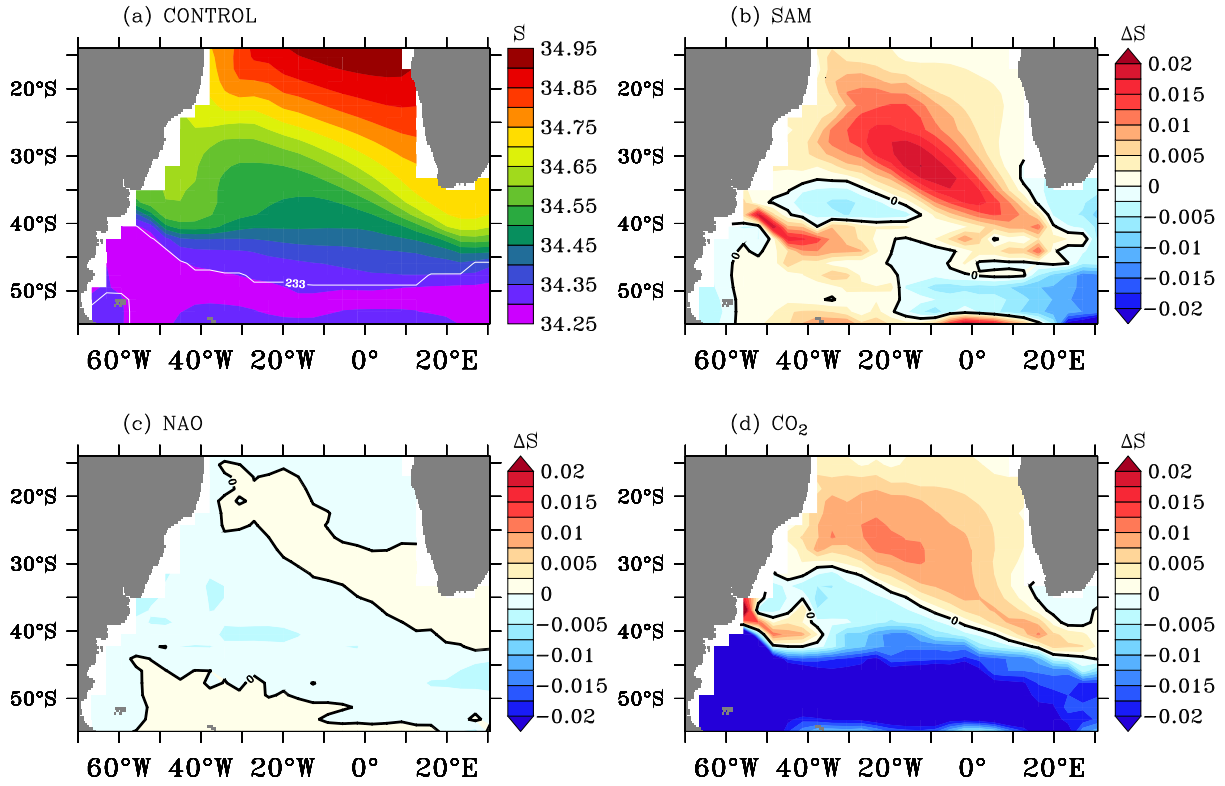
Figure 11. (a) South Atlantic salinity minimum in the Uvic CONTROL experiment averaged between 2000–2009. (b–d) Average (2000-2009) salinity minimum differences among the experiments, in which each panel shows how adding one forcing changes the salinity in comparison to the experiment without that forcing, for (b) SAM, (c) NAO, and (d) CO_2.
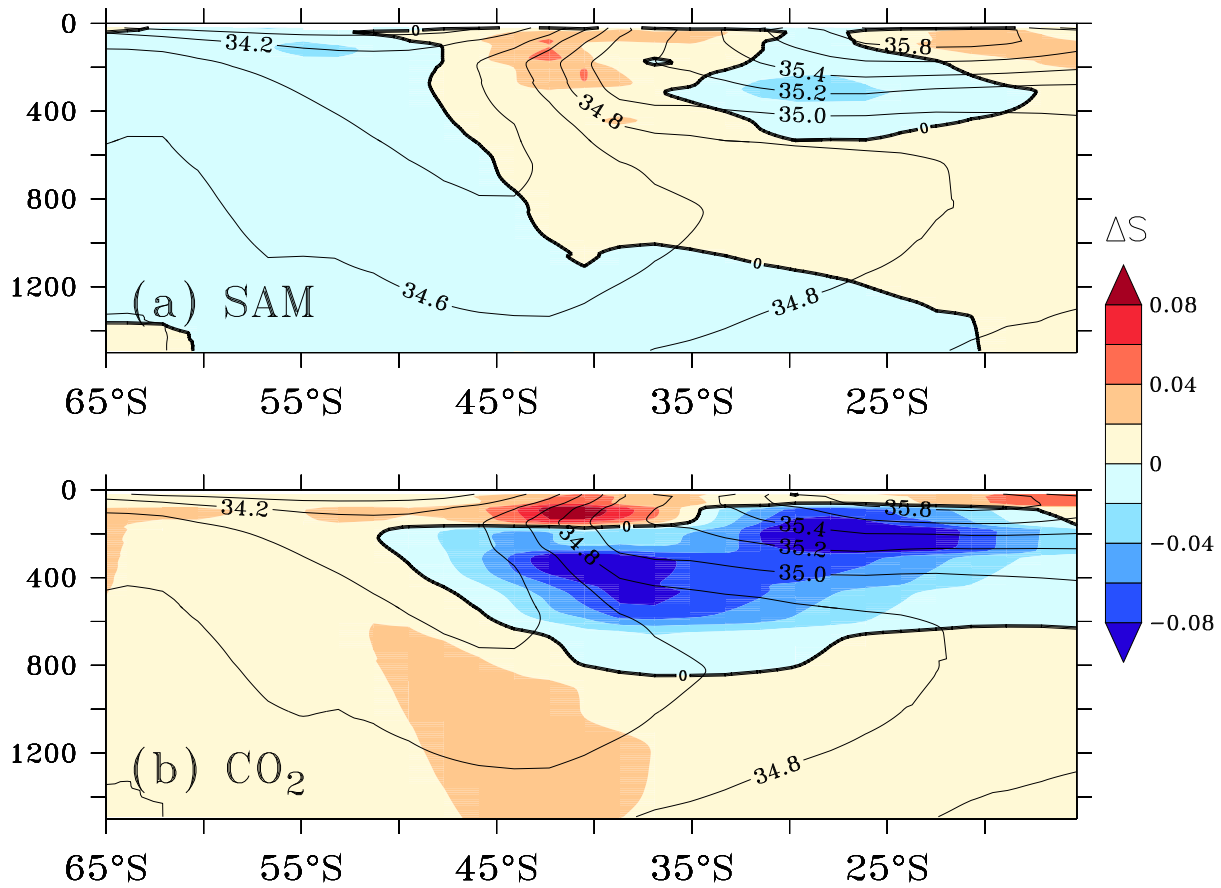
Figure 12. Meridional sections of salinity anomalies (psu) in the Atlantic Ocean for the period 2000 to 2009 for the UVic experiments forced by (a) SAM and (b) CO_2. Overlaid black contours are the sigma-averaged salinity in the section. The salinity anomalies are differences along isopycnals that have been remapped to depth levels.
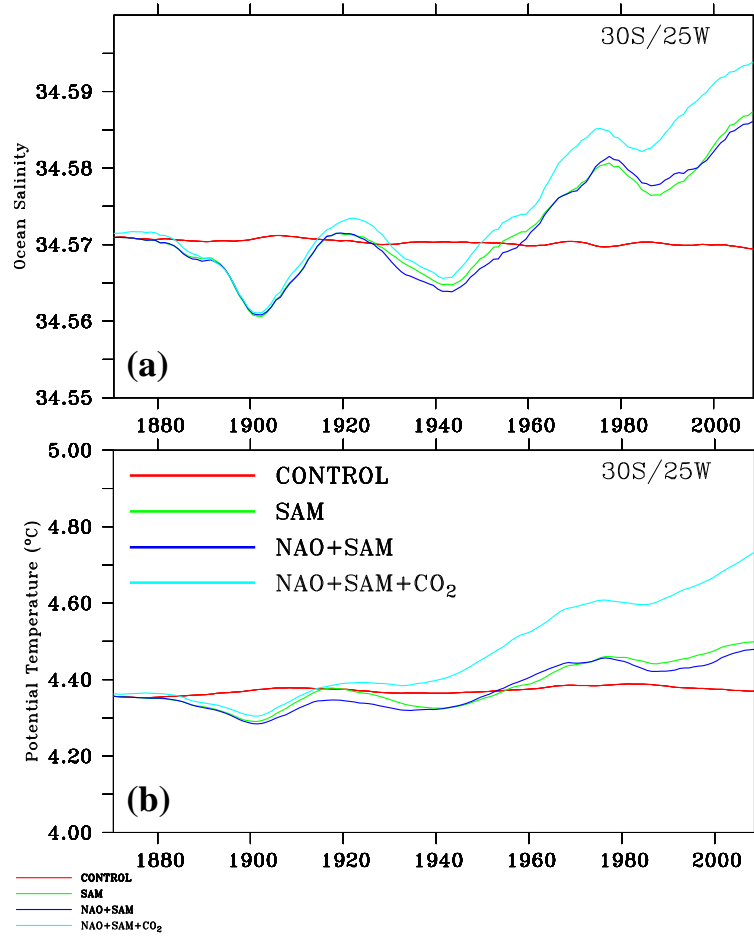
Figure 13. Time series of (a) salinity and (b) potential temperature at the salinity minimum depth at 30°S/25°W from the UVIC model experiments. The colored lines are for the CONTROL (red), SAM only (green), SAM plus NAO (dark blue), and NAO plus SAM plus CO_2 (cyan) experiments.
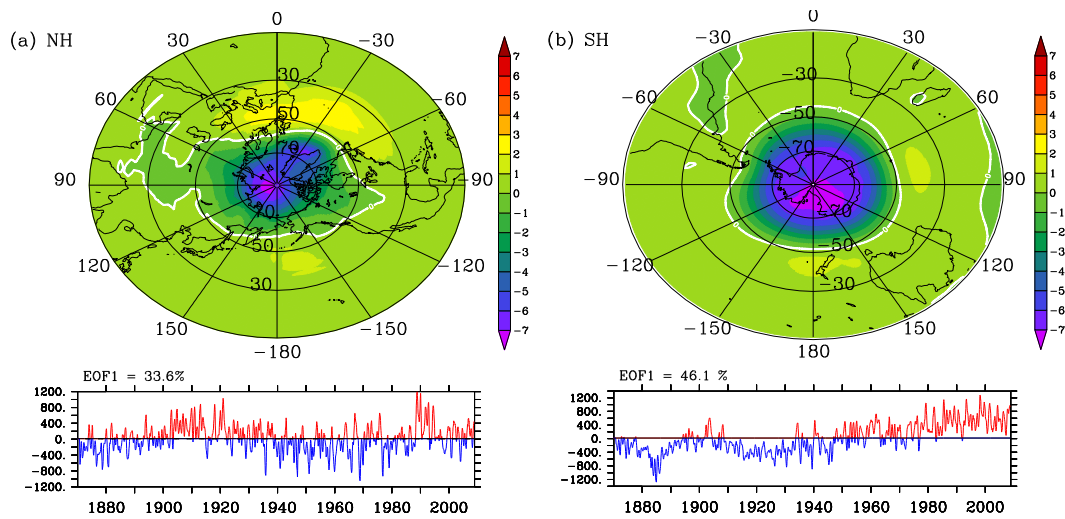
Figure 14. First EOF of the hemispheric sea level pressure used to force the atmospheric model in UVic for the (a) Northern Hemisphere and (b) Southern Hemisphere.